The wind-induced dynamic load on high-rise structures by the use of CFD

A.M. Aarts

TU Delft

abt

The wind-induced dynamic load on high-rise structures by the use of CFD

By

A.M. Aarts

in partial fulfilment of the requirements for the degree of

Master of Science

in Civil Engineering

at the Delft University of Technology,

to be defended publicly on March 12, 2021 at 2:00 PM.

Thesis committee:	Prof. Dr. A.V. Metrikine	TU Delft
	Ir. S. Pasterkamp	TU Delft
	Ir. S. Sánchez Gomez	TU Delft
	Ir. R. Roijakkers	ABT B.V.

An electronic version of this thesis is available at http://repository.tudelft.nl/.

TU Delft

abt

Preface

In this master thesis, the wind-induced load on high-rise structures by the use of CFD is explored. I experienced my research as very challenging and interesting, and I am proud of the result. This thesis was the final project of my Master Structural Engineering at the faculty of Civil Engineering and Geosciences at the Delft University of Technology.

First of all, I would like to thank engineering company ABT B.V. for giving me the opportunity to finish this research. Together we came to the topic, and gradually we converged to the final base of my research. The collaboration with multiple employees was very helpful and instructive. I especially want to thank Rudi Roijakkers for guiding me through the process. Even when you were very busy, you always would find time to help me. Our countless meetings where we discussed my progress were incredibly helpful, you wanted to understand everything and helped and motivated me when I struggled to book progress. You also checked my work regularly, which definitely lifted the quality of my work.

This thesis could not have been written without my other supervisors' feedback: I would like to thank Sergio Sánchez Gómez for his critical view. Also, I want to thank Sander Pasterkamp for keeping an eye on the bigger picture when I was focussing on smaller details. Finally, I want to thank Andrei Metrikine for his scientific approach and critical notes during my progress meetings.

After finishing this thesis, my time as a student in Delft comes to an end. I want to thank my friends for the time we spent together. Also, I am very grateful for the support of my family; you were always there and gave me the opportunity to develop myself in my educational and personal life, I could not have done this without you.

A.M. Aarts

Leiden, March 2020

Summary

During the last decades, the development of high-rise increased quickly. When the height of the structure increases, the wind loading becomes more and more substantial. The Eurocode is frequently used to make wind calculations. To make those calculations, the dynamic wind load is simplified to a conservative equivalent static load. An alternative to calculate wind loads is a physical wind tunnel test. Wind tunnel tests are expensive, time-consuming, and these tests' results cannot be reused if the design of the building changes. An alternative for these methods is the use of Computational Fluid Dynamics(CFD). CFD makes it possible to simulate the wind, but it is expensive to make accurate calculations. At this time, CFD is still very user-dependent and therefore it is stated in the Eurocode that CFD simulations cannot be used as a design tool. This research aims to examine the impact of different parameters in evaluating the dynamic loading on a high-rise structure by the use of CFD. The results of the CFD simulations are compared with a spectral approach. The spectral approach is a method that works with a wind spectrum depending on the location of the structure. The properties of the building are included in the so-called aerodynamic admittance. Combining the aerodynamic admittance with the wind spectrum results in a load spectrum. The load spectrum shows the load on the structure per wind frequency.

The Navier Stokes (NS) equations are the basics for CFD. Different models, such as Reynolds-averaged Navier-Stokes (RANS), Large Eddy Simulation (LES) and Direct Numerical Simulation (DNS) are used to solve the NS equations. The costs of CFD increase exponentially with demanding more accuracy. An extension of the RANS model is used in this research: the Unsteady-RANS(U-RANS) model. Where the RANS model only computes the steady-state solution in a simulation, the U-RANS captures the slow turbulences as well. For the objective of a dynamic wind load on a high-rise structure the slow turbulences are of more importance than the faster turbulences, since faster turbulences are balanced out within the structure. Especially the frequencies close to the natural frequencies of the structure are important. The CFD simulations are performed using Star CCM+ by Engineering Company ABT BV.

A reference structure is used to validate the CFD simulation procedure with existing available wind tunnel data of the Tokyo Polytechnic University. The wind tunnel data contains dimensionless pressure coefficients on several locations on the model. The results show a lot of noise, which is visible when the time domain's pressure coefficients are translated into the frequency domain. A dominant peak is observed at a frequency of 10 Hz, but other frequencies are triggered as well. The CFD simulation for the same reference block show less fluctuating results than the wind tunnel data: the results are only fluctuating on one frequency of 12 Hz. For this study, no further improvements are added to the CFD simulations.

Afterwards, a case study is used to compare CFD results with a spectral approach. A high-rise structure of 40 x 40 x 200 meters is used for this study. The results of the spectral approach are compared with existing literature using the structural factor $c_s c_d$. The results coincide. Several CFD simulations are performed on the same model. First, a semi 2D simulation is executed, and after that, 3D simulations are performed. The result over time converges to a constant oscillating pattern, which looks promising. The absolute values of the peak velocity pressure are of the same order of magnitude, with a difference of 10 to 25 percent. However, the values of the standard deviation differ more substantially. One of the reasons for these differences can be found in defining the extracted values at a height of 150 meters. The CFD simulation stores the average pressure over an area of 10 x 10 meters, which balances out some fluctuations. Furthermore, it can be concluded that the CFD

simulations underpredict the absolute values of the pressure consistently compared to the spectral approach.

It can be concluded that the CFD simulations require exact defined input values. The input parameters regarding the wind velocity should be changed to compare the results more appropriately to the spectral approach. The area of the averaged pressure values of 100 m^2 is too robust, reducing this area impacts in a more accurate location-dependent result.

For further research, it is recommended to validate the reference model more accurately. The U-RANS model shows too little fluctuation compared to the wind tunnel data and the spectral approach.

Symbols

Sign	Description	Unit
B^2	Background response factor	-
c_{dir}	Directional factor	-
c_e	Exposure factor	-
c_O	Orography factor	-
C_p	Pressure coefficient	-
c_r	Roughness factor	-
$c_s c_d$	Structural factor	-
C_z , C_y	Decay factors	-
d	Diameter	m
f_L	Dimensionless frequency	-
I_v	Turbulence intensity	-
k_p	Peak factor	-
k_r	Terrain factor	-
k	Turbulent kinetic energy	J/kg
L	Characteristic wind gust length	m
n	Frequency	Hz
p	Pressure	Pa
q_p	Peak velocity pressure	Pa
q_μ	Mean pressure	Pa
q_σ	Standard deviation of the pressure	Pa
R^2	Resonance response factor	-
Re	Reynolds number	-
Sr	Strouhal number	-
t	Time	s
$v_{b,0}$	Fundamental value of the basic wind velocity	m/s
v_b	Basic wind velocity	m/s
v_m	Mean wind speed	m/s
z_0	Roughness length	m
Φ	Eigenmode	-
η	Generalised coordinate	-
κ	Von Karman constant	-

Contents

Introduction

For long times buildings were designed without taking wind into account, because those first built buildings had low slenderness, so a low height over width ratio, and therefore the dead load was substantially bigger than the horizontal load caused by wind. For this reason, the wind load was not taken into account at all, but while the construction techniques were developing, the buildings started to get higher and more slender.

During the last decades, the development of high-rise increased quickly. In Western Europe, and especially in the Netherlands, high-rise development has been slower as compared to other countries. In principle the space in historical cities is limited, new buildings and high-rise buildings would pollute the skyline to some opinions.

When in the 1960s historical buildings were demolished to replace them with modern high-rise buildings, the resistance of people increased even more. In those days the population growth in the rural areas was larger than the growth in cities, so the need was smaller. Nowadays the Netherlands have become more urbanised and the demand for both residential and office buildings increases rapidly.

As a result of limited land availability, a logical solution has been to expand the buildings in height. Hence, engineers have been challenged to innovate in developing new methods to reach higher elevations efficiently. The Netherlands have an extra challenge due to the relative soft soil conditions. With an increasing slenderness, the governing load changes. The horizontal wind load gets more substantial and causes a rotation on the building. A calculation of the wind load can be made using the Eurocode 1-4(Standard, 2005). This code provides a simplified calculation of the wind loading on structures, assuming it as an equivalent static load. This simplified calculation procedure is seen as a conservative, and thus a safe manner of engineering the structure. An alternative for using this procedure is a wind tunnel test. A wind tunnel test is a physical test on smaller scale that shows how the wind flows around the structure and how this flow pattern is influenced by the adjacent environment. A disadvantage of wind tunnel testing is that it takes a lot of time to prepare and execute, and that the results can substantially change with a small change in building geometry.

Another possibility to get a more realistic load pattern caused by wind, is the use of Computational Fluid Dynamics(CFD). CFD solves the governing equations for fluids, like air, in a three-dimensional space by assuming a discretised domain. Currently it is stated in the Eurocode that CFD calculations cannot be used for strength calculations, since substantial research efforts are still needed to evaluate its accuracy and reliability. However, with ever increasing computational speeds and the possibility of cloud computing, the time and costs for making CFD simulations will drop. When the calculations can be used for strength calculations, it would give significant flexibility in playing with the dimensions and design of the building. This research will focus on the interpretation of CFD results.

1. Research description

1.1 Problem definition

In strength calculations, the dynamic wind loading is used as an equivalent static load. The equivalent static load simplifies the designing process while including safety margins. A designing method with a dynamic load could lead to a less conservative design in the end. However, safety should be guaranteed at all times.

The wind is an extremely complex phenomenon, and at the moment it is hard to give a well-detailed estimation of the wind loading in the early design phase. This is mainly because the building's shape and dimensions have a significant impact on wind behaviour, especially at local areas. Changing the dimensions could lead to a substantial reduction of the total horizontal loading. Use of The Eurocode can give a conservative indication of the equivalent static loading, but the Eurocode also states that a wind tunnel test could provide the final loads . Physical wind tunnel tests are expensive, time-consuming, and the results cannot be reused if the design slightly changes.

An alternative for the physical wind tunnel test could be the use of Computational Fluid Dynamics(CFD). CFD makes it possible to simulate the wind, but accuracy is expensive. A feasible simulation requires simplifications in simulating the problem. The drawback of CFD at the moment is that it is still very user-dependent due to different discretization methods, applying boundary conditions and numerical procedures (Y. Tamura & Kareem, 2013) and can therefore not be trusted at all times. The use of CFD as a design tool still needs substantial research effort to evaluate the accuracy and reliability (Ricci, Patruno, Kalkman, de Miranda, & Blocken, 2018). That is why it is stated in the Eurocode that CFD simulations cannot be used for strength calculations. Different types of CFD simulations are available, and for this research is only the U-RANS method used.

1.2 Aim of the research

This research aims to create a validation methodology for the reliability of CFD results. This aim leads to the following main research question:

What is the impact of various parameters in an analyse of the dynamic loading on a high-rise building resulting from wind loading by using CFD simulations?

This main question is divided into several sub-questions:

- *What assumptions have been made and which output is needed from CFD simulations?*
- *How do the CFD results have to be validated?*
- *How can the CFD results be compared with a turbulence spectrum approach?*

To achieve this aim, the following objectives are set:

- To gain relevant background information on aerodynamics around buildings
- To define which output is needed from the CFD computation
- To create an analytical model that represents a high-rise building
- To validate this model with existing literature

- To compare the CFD results with a turbulence spectrum approach

1.3 Methodology

To develop a methodology to validate the CFD results, several things need to be done. First of all, CFD results will be provided by general CFD experienced employees of the engineering company ABT B.V. To validate whether the CFD results can be trusted, a methodology must be developed to compare these results with a spectral approach. This methodology will be formed by an extensive literature review about spectral approaches and validations of CFD results. The outcomes of simulations will also be compared with the alternative method, using the theory behind the provided Eurocode for wind loads in the Netherlands. This is schematized in Figure 1.1.

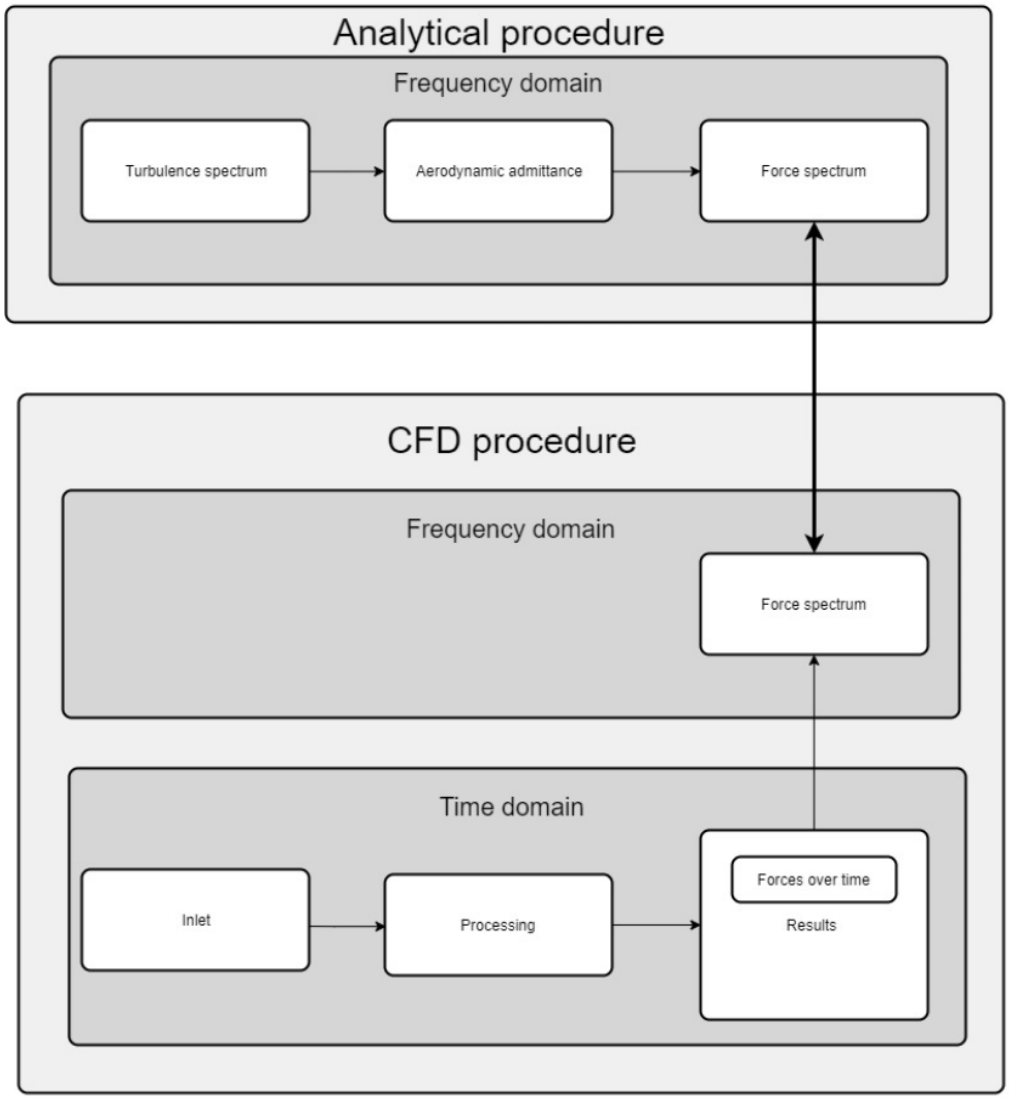

Figure 1.1. Schematic overview of the comparison between a spectral approach and CFD results

Literature review

2. Wind loading

In this chapter the basic principles of wind engineering are presented. These basics are needed to understand what steps will be taken during this research.

2.1 Basic description of wind

The atmosphere

Wind can be described as the motion of air with respect to the earth's surface. This movement is mainly caused by solar radiation, which is the strongest at the equator. The difference in the intensity of solar radiation causes temperature differences, which in turn result in pressure differences that lead to atmospheric circulations. Besides that, there are seasonal effects, geographical effects and the rotation of the earth that contribute to the variations of the wind.

Due to the variation in direction and speed, the wind is described in statistical terms. The wind movement can be separated into two main components, namely the mean wind speed and the fluctuating wind component. The mean component is chosen in a direction so that the mean components in other directions are equal to zero. However, the fluctuating component does have three directions. An example of the variation of wind over time in one direction is shown in Figure 2.1. Here, as in the Eurocode, a period of 10 minutes is taken. During these 10 minutes, a mean value can describe the wind velocity, with a fluctuation around that mean value which causes a dynamic wind load. For wind models, the extreme mean wind speed is used.

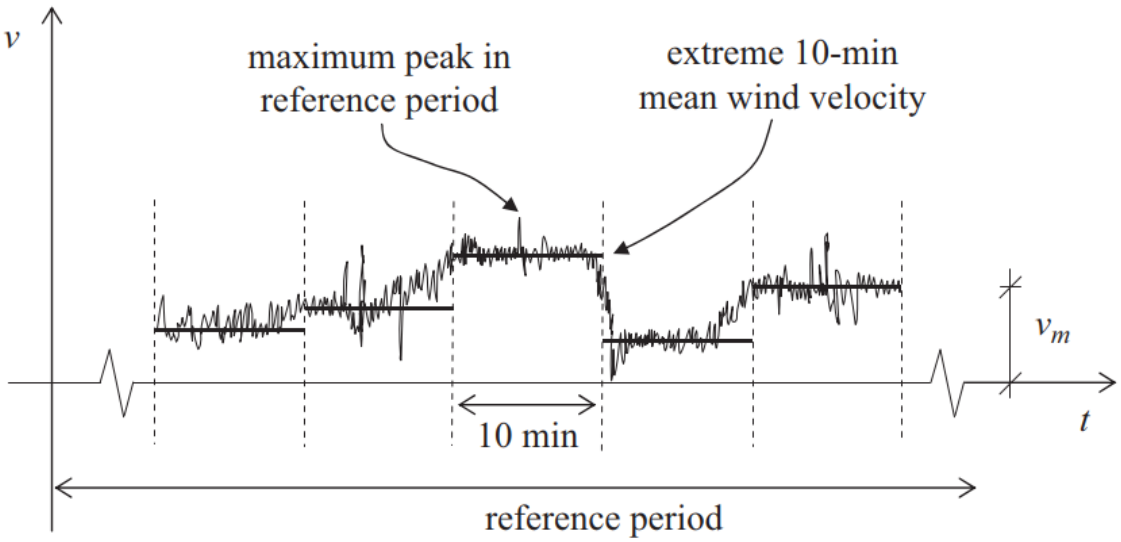

Figure 2.1. Wind velocity as a function of time (Steenbergen, Vrouwenvelder, & Geurts, 2012a)

A representation of the wind statistics can be given by the generally adopted wind spectrum by Van Der Hoven, as shown in Figure 2.2. This spectrum represents how the variance of the power spectrum is distributed over different wind periods. Two peaks can be clearly observed. The first peak is the so called mesometeorological peak at a period of around 4 days, related to the global circulation movement. The second peak is the micrometeorological peak at a period of around 1 minute and related to the turbulence caused by the topographic effects and the local surroundings around the site. The wind fluctuation in the micrometeorological peak

is associated with turbulence and therefore of importance for the dynamic wind forces in building design. (Y. Tamura & Kareem, 2013)

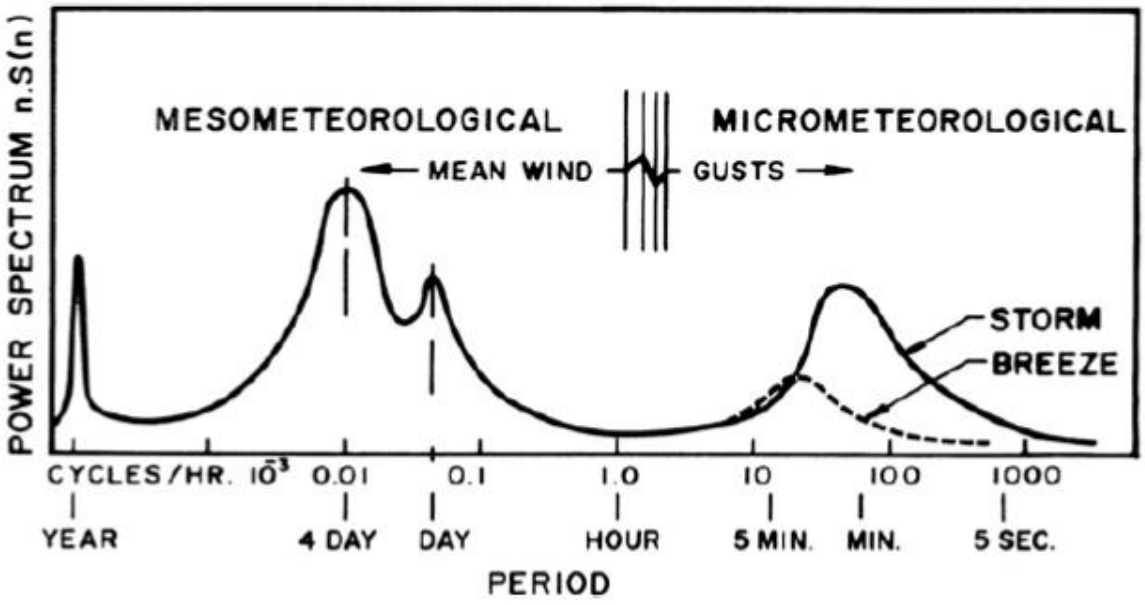

Figure 2.2. Wind spectrum by Van Der Hoven (1957) (Ted Stathopoulos, 2007)

The micrometeorological peak from the wind spectrum that represents the turbulence can be plotted in a smoothed form. Various models have been developed to describe this from, and one of the first models was developed by Davenport(Zielińska & Zarychta, 2015). This is explained in the paragraph Turbulence.

Davenport also schematized how specific aspects of wind engineering influence each other in his so called loading chain for a specific structure, as shown in Figure 2.3. The wind climate represents the kind of wind that is taken into account, for example thunderstorms or tornadoes. The influence of the terrain involves the surrounding hills and roughness's such as other buildings. The aerodynamic effects characterise the flow around the building, which makes the distinguish between a smooth or a turbulent flow pattern. Dynamic effects represents the dynamic behaviour of the building. This loading chain is directly used in the Eurocode. The wind climate, influence of terrain, aerodynamic effects and dynamic effects are captured in v_b, c_e, c_f, and $c_s c_d$ respectively.

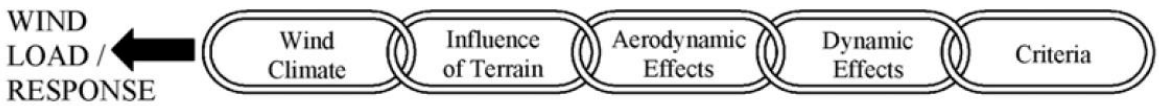

Figure 2.3 Davenport wind loading chain ("Announcement of the Alan G. Davenport Wind Loading Chain," 2011)

The statistical description of the wind

It is of importance to make a distinction between the short- and long-term distribution of the wind description. The hourly-averaged wind speed is considered to be the long-term distribution, also known as the mean wind speed. Within the term mean wind speed, an important distinction is made between the instantaneous and the extreme value. The

instantaneous mean wind speed is the mean of a certain smaller period, typically the wind speed in an arbitrary hour. The extreme value is the largest mean wind speed in one hour or the whole design lifetime. For strength calculations regarding wind the maximum wind speed during the lifetime of the structure is taken. This maximum wind speed is calculated by using the Gumbel distribution over the maximum hourly averaged extremes during each year.

The Atmospheric Boundary Layer

High above the ground the wind is independent of the friction caused by the ground surface, this higher level has so-called friction free wind. The layer from the ground surface to the boundary for this friction free wind is called the Atmospheric Boundary Layer (ABL). For describing the mean horizontal wind profile near the ground there are in general two adopted methods. The first one is the logarithmic law, as shown in (2.1).

$$v_m(z) = \frac{1}{\kappa} \cdot u_* \ln\left(\frac{z-d}{z_0}\right) \qquad (2.1)$$

Another law that also often is used is the power law in (2.2).

$$v_m(z) = v_m(z_s) \cdot \left(\frac{z-d}{z_s}\right)^{\alpha} \qquad (2.2)$$

Where

$v_m(z)$ = mean wind speed at height z.

κ =Von Karman constant, with a typical value of 0.4.

u_* = shear velocity, defined as $u_* = \sqrt{\tau_0/\rho}$, with τ_0 the shear stress at ground surface and ρ the density of air.

d = average height of the buildings.

z_0 = roughness length.

The division between both the power law and the logarithmic law can be seen in the mean wind speed profile. Figure 2.4 shows the Logarithmic law in the profile for the inner Atmospheric Boundary Layer (ABL), while the Power law describes the outer ABL.

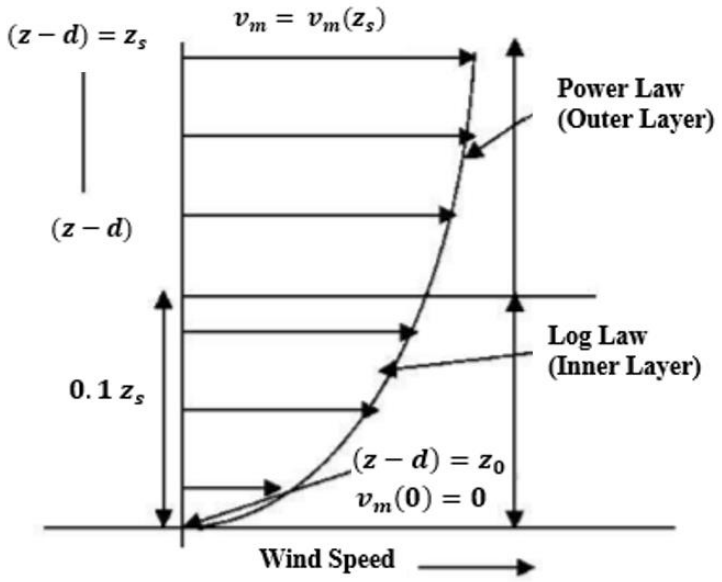

Figure 2.4. Logarithmic law and power law region in the mean wind speed profile of the atmospheric boundary layer (Abubaker, Kostić, & Kostić, 2018)

Turbulence

Next to the mean wind speed there is also the fluctuating component, which is called the turbulence. Turbulence can be generally described in three phases. The first phase is the production range, here large eddies are generated due to deviations of the mean wind. In the inertial subrange the large eddies break off to smaller and smaller eddies, this goes proportional to $log\ (K^{-\frac{5}{3}})$ for several models. In the dissipation range the viscosity becomes predominant and dissipates the energy. This is shown in Figure 2.5.

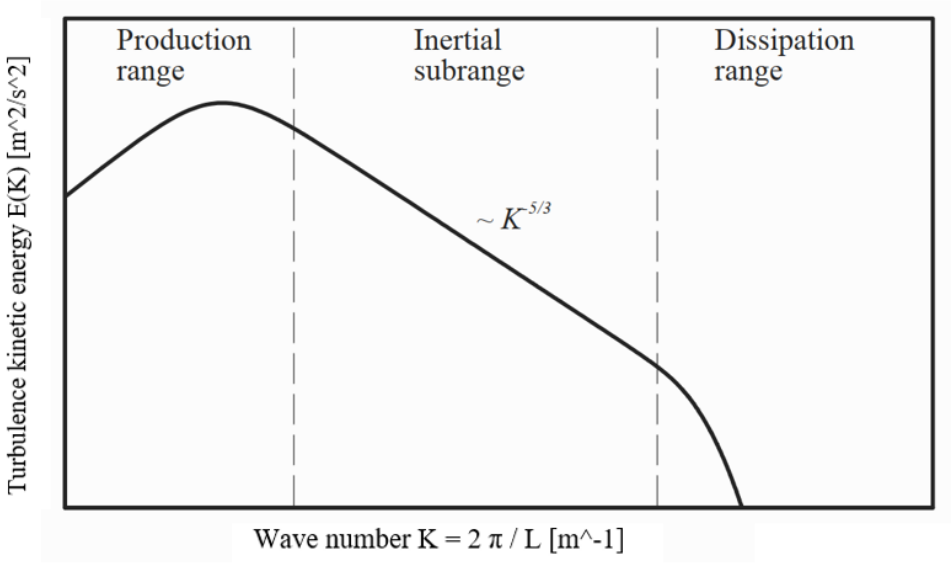

Figure 2.5. Turbulence energy spectrum (Ted Stathopoulos, 2007)

Turbulence can also be described by the turbulence intensity $I_v(z)$, defined as the ratio of the standard deviation of the wind speed to the mean velocity.

$$I_v(z) = \frac{\sigma_v(z)}{v_m(z)} \tag{2.3}$$

Where $\sigma_v^2 = \frac{1}{T}\int_0^T v^2\, dt$ for the direction v.The total standard deviation of the fluctuating speed can also be obtained by:

$$\sigma_v^2 = \int_{-\infty}^{\infty} S_{vv}(f)\, df \tag{2.4}$$

Where $S_{vv}(f)$ is the variance spectrum of the wind. This spectrum is also called the turbulence spectrum and represents the dependence upon wave number of the energy contributions of different eddies. There are several power spectra such as the Davenport's (1967), Harris' (1968), Simiu's (1975) and Solari's (1993) spectra, presented in Figure 2.6. All the spectra are approximately described by empirical formulas based on historical measurements on various locations(Zielińska & Zarychta, 2015). The shape of the turbulence spectrum does not depend on the height, but is used in multiple wind load codes to get to a wind profile over height of the turbulence intensity, the Eurocode uses the Solari Spectrum.(Y. Tamura & Kareem, 2013) (Simiu & Scanlan, 1986)

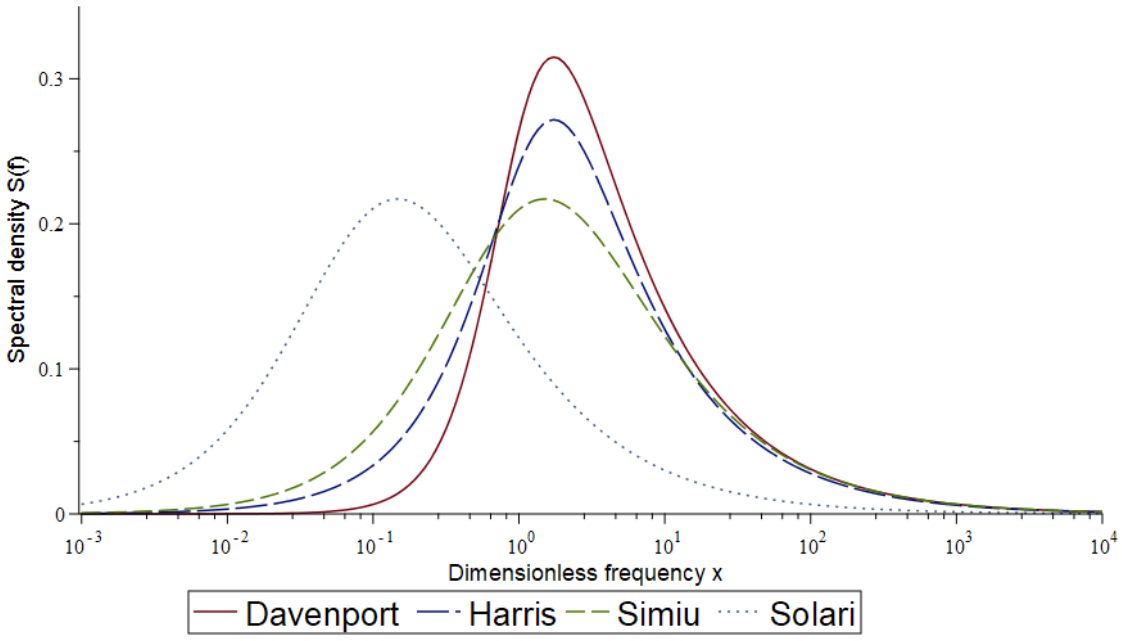

Figure 2.6. Spectra of Davenport, Harris, Simiu and Solari

The complete calculation procedure is schematised in Figure 2.7. The wind velocity profile is translated to a turbulence spectrum and by combing this spectrum with the aerodynamic properties of the structure, it can be transformed to a force spectrum. By the use of a mechanical admittance function, including the dynamic stiffness and damping properties of the structure, the response spectrum with movements can be calculated. Especially for high-rise structures is it important to check if the comfort requirements are met at all times at all locations within the building.

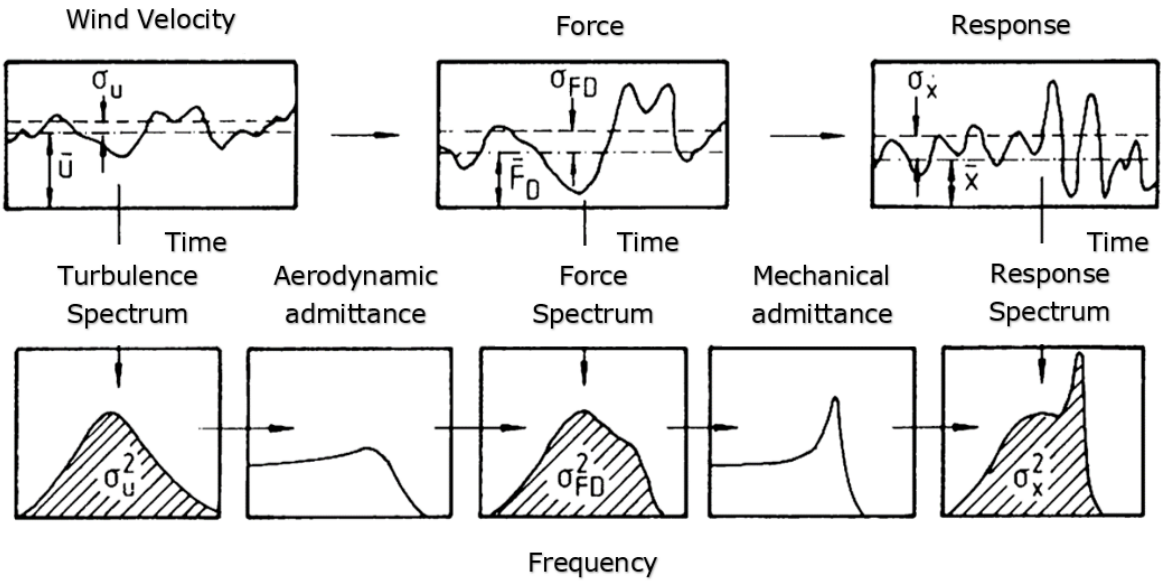

Figure 2.7. Wind excitation and response process after Davenport (Y. Tamura & Kareem, 2013)

2.2 Eurocode

The Eurocode is the European standard where is specified how a structural design should be performed. For this research the part regarding actions on structures, caused by wind, is mainly of importance, stated in *'EN1991-1-4, Eurocode 1: Actions on structures – part 1-4: General actions – Wind actions (Standard, 2005)'*. This specific part will be referred to when the Eurocode is mentioned.

As underlying principle Davenports loading chain, shown in Figure 2.3, is used to define the wind load calculation procedure. This chapter will therefore be presented according to Davenports categories. In the end the calculations procedure will result in a wind force on a structure, given by Equation (2.5).

$$F_w = c_s c_d \cdot c_f \cdot c_e(z) \cdot q_b \cdot A_{ref} \qquad (2.5)$$

Basic wind velocity v_b

The basic wind velocity is used to calculate the mean wind velocity, as stated in Equation (2.6).

$$v_m(z) = c_r(z) \cdot c_0(z) \cdot v_b \qquad (2.6)$$

$c_O(z)$= the orography factor, which takes, into account the terrain orography, such as hills or surrounding buildings.

$c_r(z)$ = the roughness factor, given by Equation (2.7).

$$c_r(z) = k_r \cdot \ln\left(\frac{z}{z_0}\right) \qquad (2.7)$$

k_r = the terrain factor, given by Equation (2.8)

$$k_r = 0{,}19 \cdot \left(\frac{z_0}{z_{0,II}}\right)^{0{,}07} \qquad (2.8)$$

v_b = the basic wind velocity defined as a function of direction and time of the year at a fixed 10 meters above ground level in terrain category II ,calculated by Equation (2.9).

$$v_b = c_{dir} \cdot c_{prob} \cdot c_{season} \cdot v_{b,0} \quad (2.9)$$

c_{dir} = the directional factor given in the National Annex.(Standard, 2005)

c_{prob} = the probability factor, taking the probability p for a yearly exceedance of the 10 minutes mean wind velocity.

c_{season} = the seasonal factor given in the National Annex. (Standard, 2005)

$v_{b,0}$ = the fundamental value of the basic wind velocity, the 10 minutes characteristic at 10 meters above ground level in terrain category II. This value can be found in the National Annex.

Exposure factor c_e

The ratio of the peak velocity pressure over height over the basic velocity is expressed as the exposure factor and is height-dependant.

$$c_e(z) = \frac{q_p(z)}{q_b} = [1 + 7 \cdot I_v(z)] \cdot c_r(z)^2 \cdot c_O(z)^2 \quad (2.10)$$

$q_p(z)$= the peak velocity pressure over the height and q_b as the basic velocity pressure is given in Equation (2.11).

$$q_b = \frac{1}{2} \cdot \rho \cdot v_b^2 \quad (2.11)$$

z_0= the roughness length, and $z_{0,II}$ is the roughness length specifically for category II. Typical values for the roughness length are presented inTable 2.1**.**

Table 2.1. Typical roughness length per category (Standard, 2005)

Terrain category		z_0 $[m]$	z_{min} $[m]$
0	Sea or coastal area exposed to the open sea	0.003	1
I	Lakes or flat and horizontal area with negligible vegetation and without obstacles	0.01	1
II	Area with low vegetation such as grass and isolated obstacles (trees, buildings) with separations of at least 20 obstacle heights	0.05	2
III	Area with regular cover of vegetation or buildings or with isolated obstacles with separations of maximum 20 obstacle heights (such as villages, suburban terrain, permanent forest)	0.3	5
IV	Area in which at least 15 % of the surface is covered with buildings and their average height exceeds 15 m	1	10

Force coefficient c_f

The force coefficient is dependent on the total structure or the structural element and its dimensions, the values are described in the National Annex.

Structural factor $c_s c_d$

The structural factor represents the non-simultaneous occurrence of peak wind pressures and the corresponding vibrations due to turbulence. The factor can be separated into a size factor c_s and a dynamic factor c_d, but is often used as the combined factor $c_s c_d$. The formula in Equation (2.12) can only be used for general shapes like rectangular shapes and when the along-wind vibration is significant in the fundamental mode.

$$c_s c_d = \frac{\left(1 + 2 \cdot k_p \cdot I_v(z_s) \cdot \sqrt{B^2 + R^2}\right)}{1 + 7 \cdot I_v(z_s)} \qquad (2.12)$$

With z_s the reference height for determining the structural factor, where for slender structures this value can be calculated with $z_s = 0{,}6 \cdot h$.

k_p= the peak factor, defined as the ratio of the maximum value of the fluctuating part of the response to its standard deviation.

$I_v(z_s)$= the turbulence intensity as mentioned in (2.3). This expression can be rewritten as a function of the turbulence factor k_I, the orography factor $c_o(z)$ and the reference height z_s, as shown in Equation (2.13).

$$I_v(z) = \frac{\sigma_v}{v_m(z)} = \frac{k_I}{c_o(z) \cdot \ln\left(\frac{z}{z_s}\right)} \qquad (2.13)$$

k_I = the turbulence factor and given in the National Annex.

B^2 = the background response factor, which allows the lack of full correlation of the pressure on the structure's surface.

R^2 = the resonance response factor, which allows turbulence in resonance with the vibration mode.

2.3 Spectral approach

A spectral approach of a wind calculation uses a wind spectrum depending on the location. Various spectra are developed over time by collecting wind statistics. In this thesis the spectrum of Solari is used, as this spectrum is used in the Eurocode as well. The wind spectrum is given and is combined with the aerodynamic admittance to create the load spectrum.

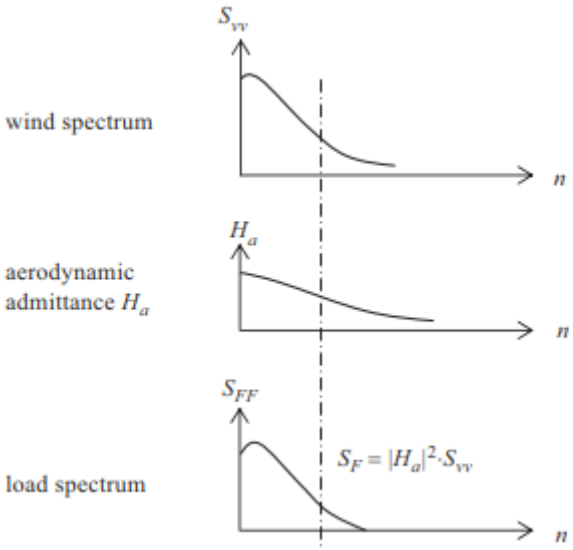

Figure 2.8. Overview of spectral approach resulting in a Load Spectrum (Steenbergen et al., 2012a)

In the different building codes, mainly static calculation formulas are presented. These static formulas include the structural factor $c_s c_d$ which is a combination of the size factor c_s and the dynamic factor c_d. The size factor takes into account the reduced effect of wind action due to the non-simultaneous occurrence of the peak wind pressures. The dynamic factor takes into account the increased effect of vibrations due to turbulence in resonance with the structure.

The theory behind these factors is based on a spectral approach, which represents the variance of the turbulence intensity over different frequencies. The structural factor $c_s c_d$ is used to compare and validate the spectral approach with results of a code mandated calculation.

Structural model

A high-rise building can be schematized and simplified to a tall building with certain dimensions. In this case, a square building with a height in the z-direction is loaded by a distributed wind load per unit area. The structure can be modelled using a *ndof* (*n* degree of freedom system) by the following coupled system of equations of motion:

$$\boldsymbol{M} \cdot \ddot{u} + \boldsymbol{C} \cdot \dot{u} + \boldsymbol{K} \cdot u = F(t) \qquad (2.14)$$

Here are $\boldsymbol{M}, \boldsymbol{C}$ and $\boldsymbol{K}$ the mass matrix, the damping matrix and the stiffness matrix respectively, based on the structural properties and dimensions of the structure. The response of the structure u is both coordinate- and time depending, where $\ddot{u}, \dot{u}$ and u are representing the acceleration vector, the velocity vector and the displacement vector. Under a dynamic load, the response u can be split in a time-dependent and a coordinate dependent component.

$$u\,(y, z, t) = \sum \eta_i(t) \cdot \Phi_i(y, z) \qquad (2.15)$$

The response of the building is now expressed in the i^{th} generalised coordinate $\eta_i(t)$ depending on time and the i^{th} eigenmode $\Phi_i(y, z)$. In Figure 2.9 the model is drawn with only one degree of freedom system (*sdof*).

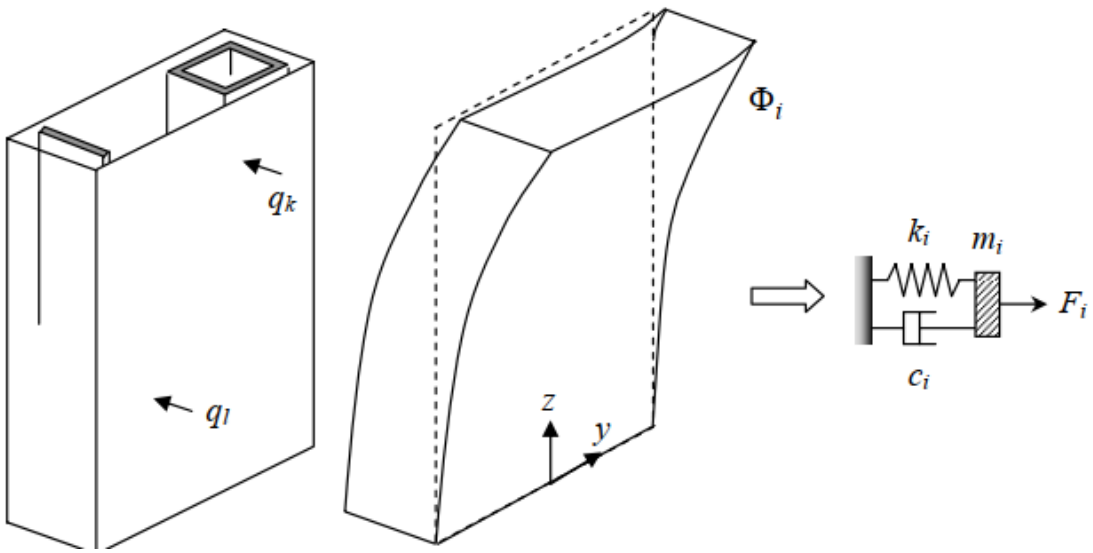

Figure 2.9. Schematic view of a high-rise building (Steenbergen, Vrouwenvelder, & Geurts, 2012b)

The *sdof* system is described by the i[th] uncoupled equation of motion as stated in Equation (2.14).

$$m_i\ddot{\eta}_i + c_i\dot{\eta}_i + k_i\eta_i = \int_h \int_b \Phi_i(y,z) \cdot q(y,z,t)\, dydz = F_i(t) \tag{2.16}$$

Turbulence spectrum

Several turbulence spectra are developed over time, in the Eurocode the spectrum of Solari is used. The dimensionless frequency $f_L = n \cdot \frac{L}{v_m}$, where n is the actual frequency, L is the characteristic wind gust length and v_m is the mean wind speed at a certain height. The vertical axis represents the power spectral density function S_L, which is a function of the variance spectrum of the wind velocity S_{vv}.

$$S_L = \frac{n \cdot S_{vv}}{\sigma_v^2} = \frac{6.8 \cdot f_L}{(1 + 10.2 \cdot f_L)^{\frac{5}{3}}} \tag{2.17}$$

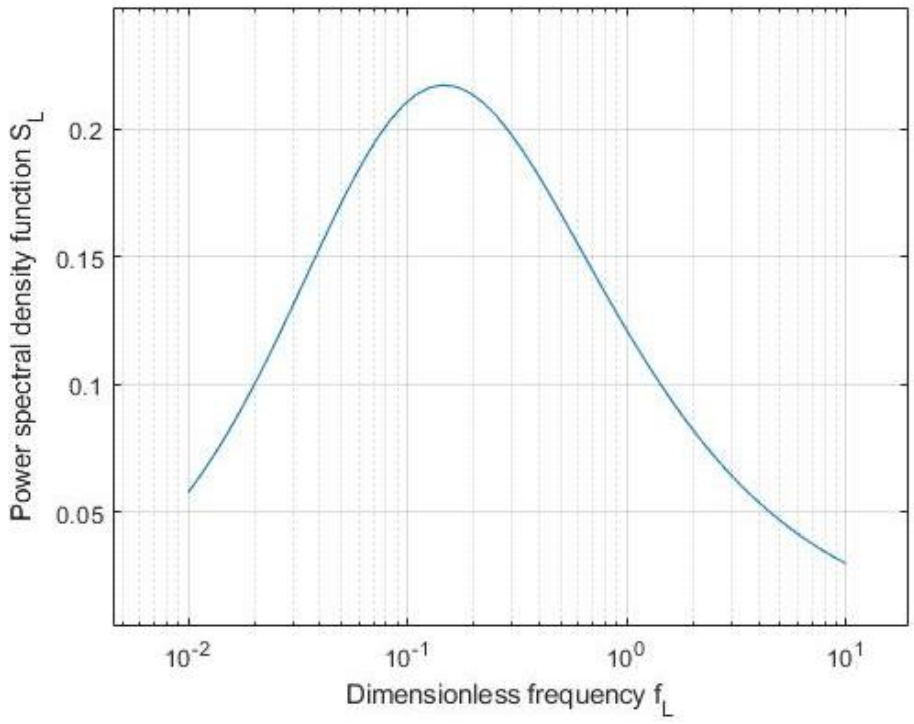

Figure 2.10 Power spectral density function of Solari

This spectral representation of the wind velocity varies over height and is therefore in general only valid for one point. For larger areas on building facades the coherence function is used. This function describes the coherence of the fluctuating wind in both space and time. (Steenbergen et al., 2012a)

Aerodynamic admittance

For the aerodynamic admittance the coherence function is of importance. This function takes into account the relation of the fluctuating wind in time and space on the structure. Here the relation between coordinate *(z_k,y_k) and* (z_l,y_l) on the façade of the building is of importance. The coherence function is still depending on the frequency *n* of the wind velocity.

$$coh_{v_k v_l}(n) = e^{\frac{-2\,n}{v_m(z_k)+v_m(z_l)}\sqrt{C_z^2(z_k-z_l)^2+C_y^2(y_k-y_l)^2}} \tag{2.18}$$

C_y and C_z represent the decay factors, which are taken according to Eurocode (Standard, 2005) as $C_y = C_z = 11.5$. When a rectangular façade is taken in account where $A = h \cdot b$, the aerodynamic admittance can be described by $X^2_{\Phi_i}(n)$.

$$X^2_{\Phi_i}(n) = \frac{1}{A^2}\int_h\int_h\int_b\int_b \frac{v_{m,k}}{v_{m,z_s}}\frac{v_{m,l}}{v_{m,z_s}}\,\Phi_i(y_k,z_k)\,\Phi_i(y_l,z_l)\,coh_{v_k v_l}(n)\,dy_k dy_l dz_k dz_l \tag{2.19}$$

The load spectrum afterwards is calculated as follows.

$$S_{FF} = |H_a|^2 S_{vv} \tag{2.20}$$

With

$$H_a(n) = \left(c \cdot \rho \cdot v_{m_{zs}} \cdot A\right) X\,(n). \tag{2.21}$$

The variance of the wind load is expressed as

$$\sigma_F = \rho \cdot c \cdot v_{m_{zs}} \cdot \sqrt{\Gamma} \cdot \sigma_{v,zs} \tag{2.22}$$

Where Γ is representing the quasi-static response.

$$\Gamma = \int_0^\infty X^2 \, \frac{S_L(n)}{n} dn \tag{2.23}$$

Load spectrum

The load spectrum can be computed with Equation (2.20). An overview of the results is presented in Figure 2.11.

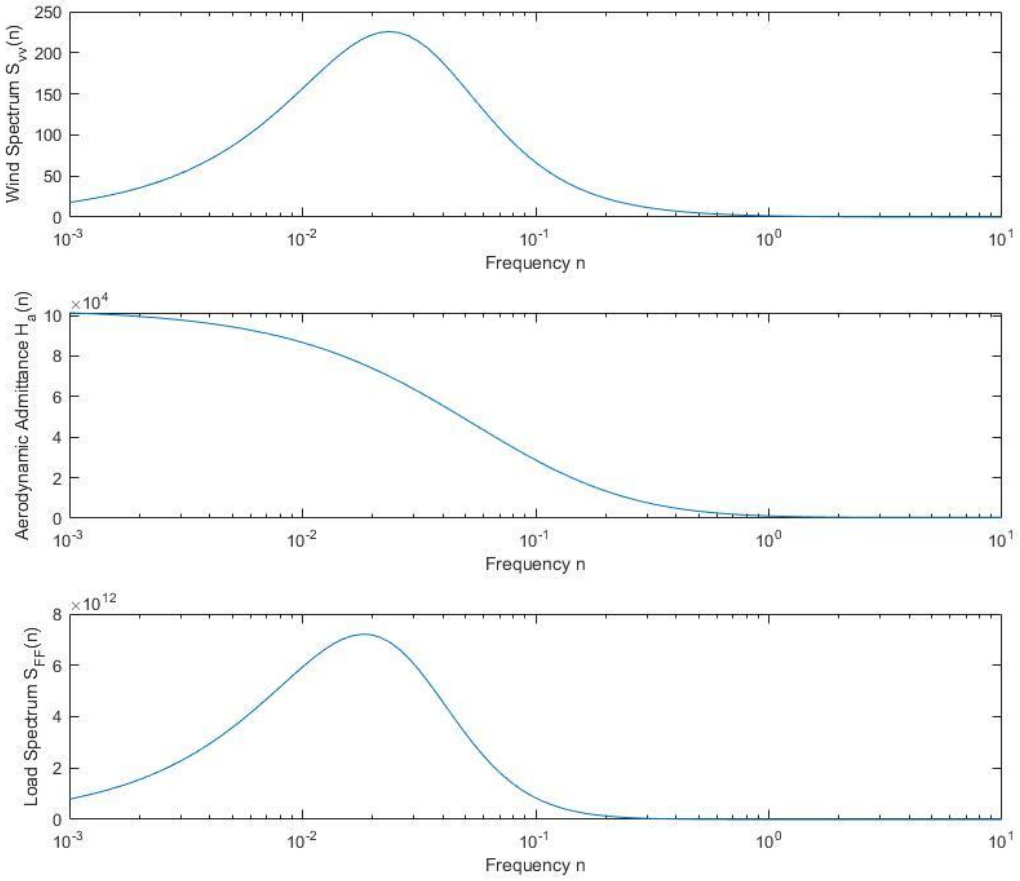

Figure 2.11. Overview of spectral approach results

Comparison with structural factor $c_s c_d$

The formulas shown in the previous paragraph are compared afterwards to the structural factor $c_s c_d$. This is done by use of the mean aerodynamic transfer $\bar{J}$.

$$\bar{J} = \frac{1}{A}\int_h \int_b \frac{c}{c_{z_s}} \left(\frac{v_m}{v_{m,z_s}}\right)^2 \cdot \Phi_i \, dy \, dz \tag{2.24}$$

The mean aerodynamic transfer is used to calculate the background response factor B^2 and the resonance response factor R^2.

$$B^2 = \frac{\Gamma}{\bar{J}^2} \text{ and } R^2 = \frac{\Upsilon}{\bar{J}^2} \tag{2.25}$$

The Υ is formulated in such a way that the wind spectrum is approximated by a white-noise spectrum intensity $S_L(n_i)$ and includes the logarithmic damping of the structural model δ_i.

$$\Upsilon = \frac{\pi^2}{2\,\delta_i} X^2(n_i) S_L(n_i) \tag{2.26}$$

The background response factor and the resonance response factor are combined with the turbulence intensity and the peak factor for the dynamic response in the following formula:

$$c_s c_d = \frac{\left(1 + 2 \cdot k_p \cdot I_v(z_s) \cdot \sqrt{B^2 + R^2}\right)}{1 + 7 \cdot I_v(z_s)} \tag{2.27}$$

$$k_p = max\left\{\sqrt{2 \cdot \ln(\nu \cdot T)} + \frac{0.6}{\sqrt{2 \cdot \ln(\nu \cdot T)}}, 3\right\} \tag{2.28}$$

$$\nu = max\left\{n_{1,x} \cdot \sqrt{\frac{R^2}{B^2 + R^2}}, 0.08\ Hz\right\} \tag{2.29}$$

Where n_{1_x} is the eigenfrequency of the structure.

2.4 Wind tunnel testing

To get a detailed view on the wind loading on and around structures, physical wind tests are often used. There are in general four types of wind tunnels: subsonic or low-speed, transonic, supersonic and hypersonic wind tunnels. For civil engineering an atmospheric boundary layer wind tunnel is the most common, this being one of the subsonic or low-speed types. (Abubaker et al., 2018)

When a physical wind tunnel test is performed, there are two techniques that are the most generally adopted. The first one is the high-frequency base balance (HFBB). The HFBB simplifies structural mode shapes, which brings uncertainties with it. However this technique is easier to perform when the design has not finished yet, and therefore is it common to use it in the early design phase. The other technique is called the high-frequency pressure integration (HFPI). The HFPI requires pressure measurement taps at several locations on the entire model simultaneously. (Luo, Liu, Xue, & Lin, 2019)

2.5 Computational Fluid Dynamics in general

Governing equations

Since the last centuries Computational Fluid Dynamics (CFD) have developed substantially and are widely used in flow-related engineering fields. CFD can be seen as a numerical approach to simulate a flow, which is done by solving a set of coupled equations. The governing equations of the CFD are the mass continuity equation and the Navier-Stokes(NS) equation, which represent the conservation of mass and the conservation of momentum respectively.

The continuity equation:

$$\frac{\partial u_i}{\partial x_i} = 0 \qquad (2.30)$$

The Navier-Stokes equation:

$$\frac{\partial u_i}{\partial t} + u_j \frac{\partial u_i}{\partial x_j} = -\frac{1}{\rho}\frac{\partial p}{\partial x_i} + \frac{1}{Re}\frac{\partial^2 u_i}{\partial x_j \partial x_j} + f_i \qquad (2.31)$$

Where u, t, p, Re and f_i are denoted as velocity, time, pressure, Reynolds number and external forces respectively. The NS equation is a nonlinear coupled differential equation. The NS equations are solved for a discretised set of points, where various difference schemes could be used. Some schemes could lead to an unstable calculation in specific cases. In case of a stable calculation process, the error that occurs depends mainly on the grid size. A higher order accuracy or a smaller grid size results in a smaller error. The stability of the calculation also depends on the Reynolds numbers in the considered domain. If no measures are taken, calculations with high Reynolds numbers usually fail. Turbulence viscosity or numerical viscosity is usually included in simulations, to dissipate the turbulent energy at high frequencies and to prevent an unstable simulation (Y. Tamura & Kareem, 2013). Different methods to solve this with computational calculations are possible. The RANS model, the LES model and the DNS model are the three different models, with an increasing accuracy in this order. This is shown in Figure 2.12. The computational costs are also exponentially increasing in the same order. Regarding the method used, assumptions have to be made to solve the NS equations.

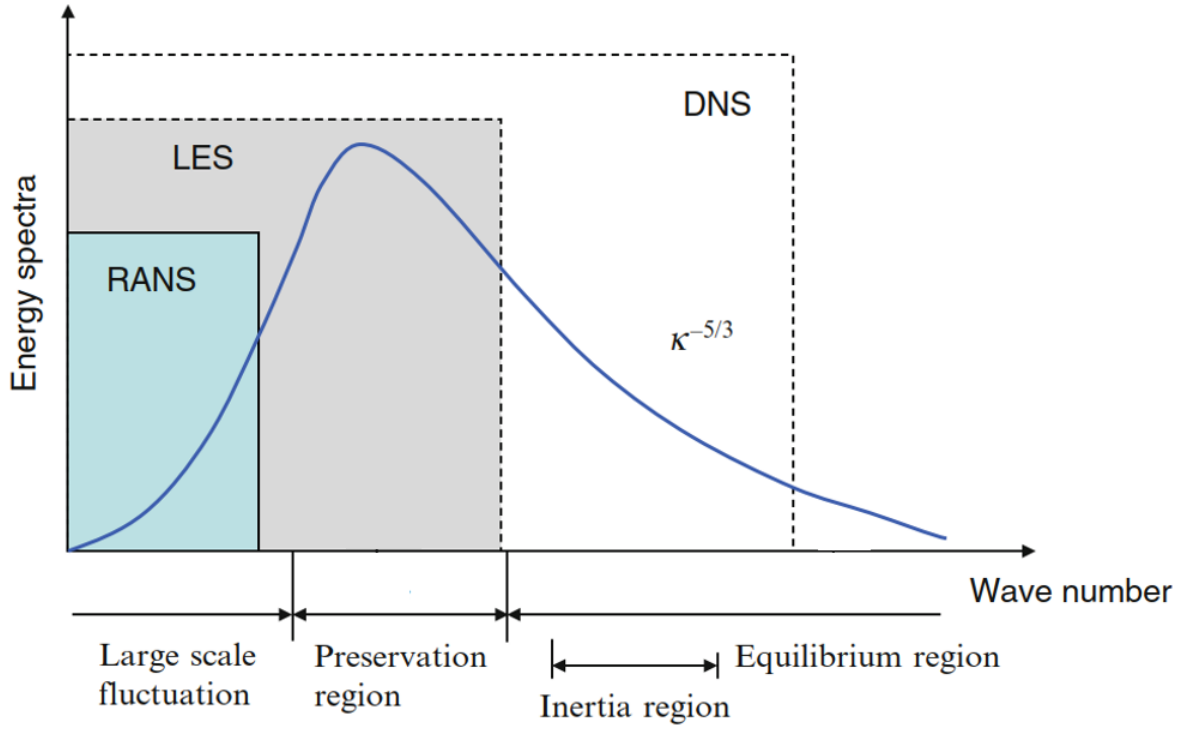

Figure 2.12. Turbulence spectrum with various models(Y. Tamura & Kareem, 2013)

Reynolds-Averaged Navier-Stokes model

Reynolds-averaged Navier-Stokes (RANS) solves the NS equations for the steady-state solution. This model has mathematically more unknowns than equations, so supplementary turbulence models are used. A more detailed description is given in the paragraph Turbulence models in Chapter 2.6.

RANS is less time consuming and less expensive method compared to the other methods, but the results are averaged over time and therefore cannot be used for dynamic calculations. An extension of the RANS method is the Unsteady RANS (U-RANS) method. U-RANS is used for transient flow calculations, the time dependent components of the results are highly depending on the time-step size of the computation. The smallest characteristic time scale of the flow has to cover the required physics. This lower limit can be found by repeating the simulation with lower time steps. When the solution converges, it can be concluded that the right physics have been captured. (Epinette & Sutton, 2003). The difference between the U-RANS and the more detailed Large Eddy Simulation and Direct Numerical Simulation is the degree of solving and modelling. The U-RANS method models kinetic energy, where the most detailed Direct Numerical Simulation completely solves the kinetic energy analytically. The Large Eddy Simulation partly solves and partly models the kinetic energy. U-RANS only captures, next to the steady state solution, the slow unsteady effects (Tominaga, 2015).

Large Eddy Simulation model

Another turbulence model is the Large Eddy Simulation (LES), which solves large scale components of the flow directly with a modelled sub-grid and can capture local unsteadiness. The LES-results for are very sensitive to the inflow conditions. The time series of the flow quantities are obtained at all grid points, this allows the evaluation of the mean values and the peak values, but also the power spectra of the fluctuations at all points. Time-dependent calculations are possible with the use of LES, but these simulations are very time-consuming because 3D calculations have to be made and long-time series of flow streams are required to achieve a reliable result. (Ricci et al., 2018)

Direct Numerical Simulation

The Direct Numerical Simulation (DNS) is theoretically perfect, but way too costly for full-scale simulations. This method captures all length and time scales of a turbulent flow directly, without making any assumptions. This requires a very fine three-dimensional grid and numerous time steps. The complexity scales with the Reynold numbers of the geometry in the assumed domain.

CFD in engineering

Although CFD has been significantly improving over the last decades due to increasing computational power and additional research, the results still cannot be used for the assessment of wind loads on structures. Especially the complex flow interference induced from buildings is difficult to model acceptably. (Clannachan, Lim, Bicanic, Taylor, & Scanlon, 2009)

2.6 Computational Fluid Dynamics modelling principles

The modelling process starts with determining the purpose of the simulation. The physical geometrical properties, the materials properties and the flow conditions are fundamental. The relevant physics have to be translated in numerical values of appropriate parameters. A

computational mesh is set up and a modelling strategy is chosen (*CCM User Guide- star- CD version 4.02*, 2006). The reality needs to be presented in a relevant model and therefor the user has to balance the requirement of reliability and accuracy against computational capacity and computational costs.

Defining the domain

An essential part of solving the NS equations is the volume discretisation. A solution domain is defined and divided in a mesh of cells. These cells are finite, discrete, continuous volume elements.

A CFD simulation requires a bounded computational domain. There are best practice guidelines available that provide the appropriate distance of the boundaries to the building of interest. The distances of the boundaries are dependent on the dimension of the building and the coherent blockage ratio. The blockage ratio is the ratio between the area of the structure(s) divided by the total area of the wind direction. For CFD simulations a maximum blockage ratio of 3% is recommended (Franke, Hellsten, & Carissimo, 2007). Different types of boundaries are available to restrict the domain, the boundaries can be roughly divided in the following types (*CCM User Guide- star- CD version 4.02*, 2006), (Franke et al., 2007):

- Physical boundaries: solid obstacles or walls provide a physical restrain of the flow.
- Symmetrical boundaries: a plane defines a mirror surface and the normal components of all variables are set to zero.
- Periodic boundaries: also known as a cyclic boundary, this type of boundary is used for repeated geometries.
- Notional boundaries: non-physical surfaces that provide closure of the solution domain in the regions not covered by the other types. The inlet- and outlet boundary conditions are the best known notional boundaries.
- Slip boundaries: assumes that the fluid flow is parallel to the wall at this point.
- No-slip boundaries: this is the most common boundary where the normal component of the boundary condition is equal to zero and the tangential component of the velocity is usually non-zero.

Mesh definition

An essential part of solving the NS equations is volume discretisation. The solution domain is defined and divided into a mesh of cells. These cells are finite, discrete and continuous elements. Numerical discretisation errors are related to the cell size; the larger the cells, the higher the errors. Nevertheless, smaller cells result in a higher mesh density, which entails higher computational costs. Mesh refinement applies a higher mesh density on locations of interest for the simulation. Since simulations can develop over time, it is possible that the areas of interest change over time. The adaptive mesh confirms the importance of the mesh refinements over time and adapts the mesh in consequence. Figure 2.13 shows an example of an adaptive mesh refinement, where the vortices are captured with a changing mesh.

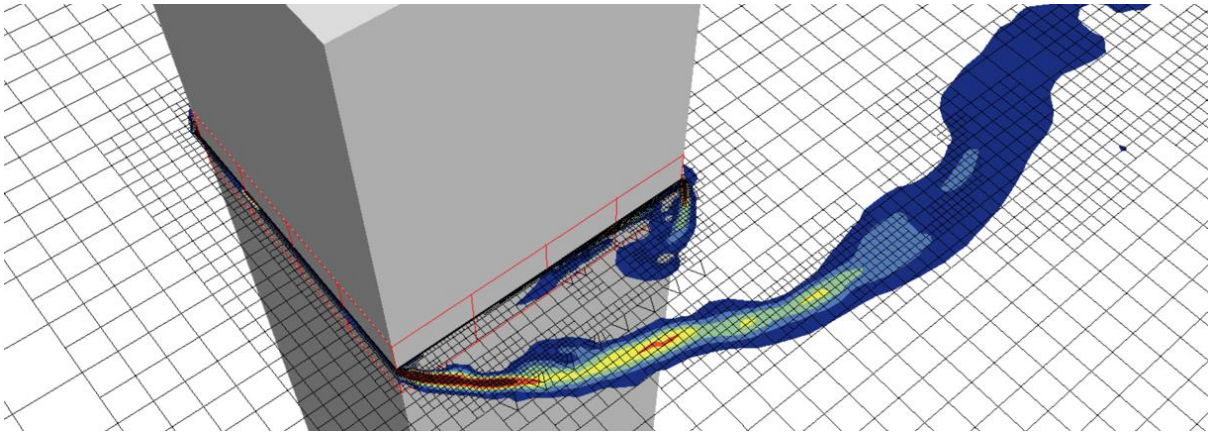

Figure 2.13 Example of an adaptive mesh refinement

Flow characterisation

Different mathematical models and numerical solution algorithms are available to solve the governing equations. The nature of the flow determines the appropriate model, otherwise, problems will occur later. The fluid's physical properties, such as density, molecular viscosity, and thermal conductivity, are required for the inlet conditions.

Turbulence models

Turbulence modelling is required when a flow enters the domain in an inlet or outlet boundary. The turbulence modelling includes production and dissipation of turbulence. When a flow is laminar, turbulence quantities are transported, but not changing. (Epinette & Sutton, 2003). The models assume various proportionalities in turbulence spectra. Dependent on the location in the assumed domain, it can vary what kind of model gives the most accurate results. A well-known model is the standard $k-\epsilon$ model, where a distinction is made between the turbulent kinetic energy k and the rate of turbulent dissipation of kinetic energy ϵ. This model isn't memory intensive and has a good convergence. The Realizable $k-\epsilon$ model is a variation on the standard model, where a modification of ϵ improves the effect of the transport of the fluctuating vorticity (Shaheed, Mohammadian, & Kheirkhah Gildeh, 2019).

Initial conditions

Before the calculations are started, all cells have values assigned for the dependent variables. These assigned starting values are known as the initial conditions. When the simulation is running, the conditions measured in the cells are solved by iterative means. Well-chosen initial conditions speed up the total simulation time. (*CCM User Guide- star- CD version 4.02*, 2006)

Modelling

3. Reference structure

Before the full-scale CFD models of high-rise buildings are built, there is a need to validate a simplified shape with existing reference data. This reference data originates from an aerodynamic database with wind tunnel (WT) test results of the Tokyo Polytechnic University. In this database are findings of multiple tests with different configurations presented (Y. (Tokyo P. U. Tamura, 2012). All results are also checked with simple hand calculations.

3.1 Wind tunnel data

The Tokyo Polytechnic University started in 2003 the 21st Century Centre of Excellence Program, including a Wind Effects on Buildings and Urban Environment section. (Tamaru & Quan, 2007). For this program multiple wind tunnel test were executed, and the results are available online. Different compositions are used, e.g. a single high-rise building, two adjacent tall buildings, an isolated low-rise building or a non-isolated low rise building. The objective of the program is to provide structural engineers with wind tunnel data on structures. The wind tunnel dataset of the Tokyo Polytechnic University is compared with other wind tunnel data (Amin & Ahuja, 2013) and the Eurocode(Standard, 2005) in Appendix D – Comparison of Wind tunnel data. Only the data from the Tokyo Polytechnic University of the single high-rise building is used for this thesis.

A total of 22 single high-rise models were tested in a wind tunnel, and these models vary in dimensions and exposure factors. The model is placed in a wind tunnel of 2.2 meters wide and 1.8 meters high. The model is positioned on a turning table, so different angles of wind loading are available. The dimensions' values are scaled with a factor of 1/400 for a reference structure of representative height. The velocity scale is 1/3. Table 3.1 shows the dimensions of the wind tunnel model and the coherent representative high-rise model.

Table 3.1 Dimensions of wind tunnel reference data

	Wind Tunnel Model	**Representative high-rise model**
Width (m)	0,1	40
Depth (m)	0,1	40
Height (m)	0,5	200
Exponent (logarithmic law)	0,25	0,25
Incoming velocity v_m (m/s)	11.1	33.3

Five hundred pressure taps with a diameter of 1 mm are placed on the reference model (Hagos, Habte, Chowdhury, & Yeo, 2014). Pressure coefficients were measured over a period of 33 seconds with a sample frequency of 1000 Hz. The first validation of the CFD simulation uses several points at a height of 0.25 meters. This height is the only one investigated since the computational time increases exponentially for CFD simulations with output over multiple elevation levels. Figure 3.1 visualises the locations of the used points on the structure and the incoming wind profile's characterisation.

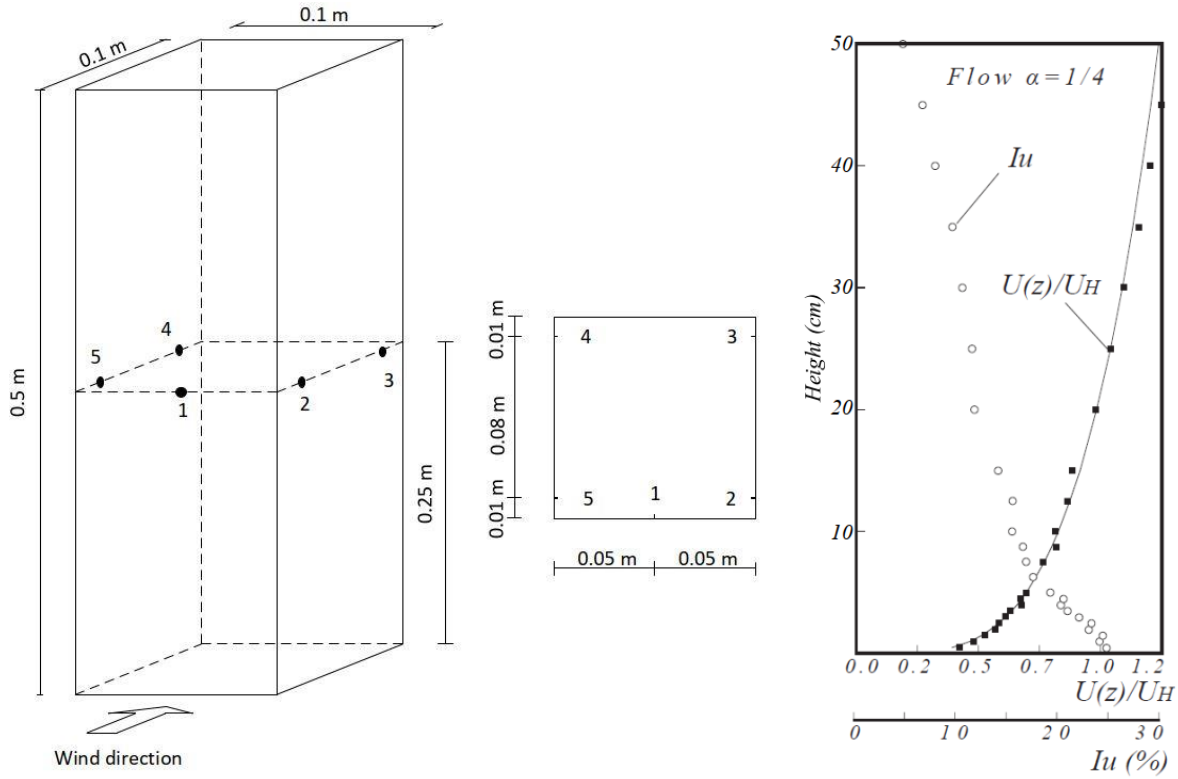

Figure 3.1 (left) Location pressure taps from wind tunnel data, (centre) Top view of location pressures taps, (right) Vertical profile of the incoming flow (Y. (Tokyo P. U. Tamura, 2012)

Equation (3.1) shows the conversion of the measured pressure values to the pressure coefficients.

$$C_p = \frac{p - p_\infty}{\frac{1}{2} \cdot \rho_\infty \cdot v_\infty^2} \tag{3.1}$$

The pressure coefficient C_p is a dimensionless number which describes the ratio of the pressure forces to the inertial forces, as shown in Equation (3.1). The pressure p is location-dependent and measured with a pressure tap. The pressure p_∞ represents the pressure in the freestream without any disturbance. The freestream velocity v_∞ here is 11.1 m/s. Figure 3.2 shows the pressure coefficients of all points of interest over the total simulated time. Figure 3.3 presents the same results but given as closeup for 0.3 seconds, starting from 20 seconds.

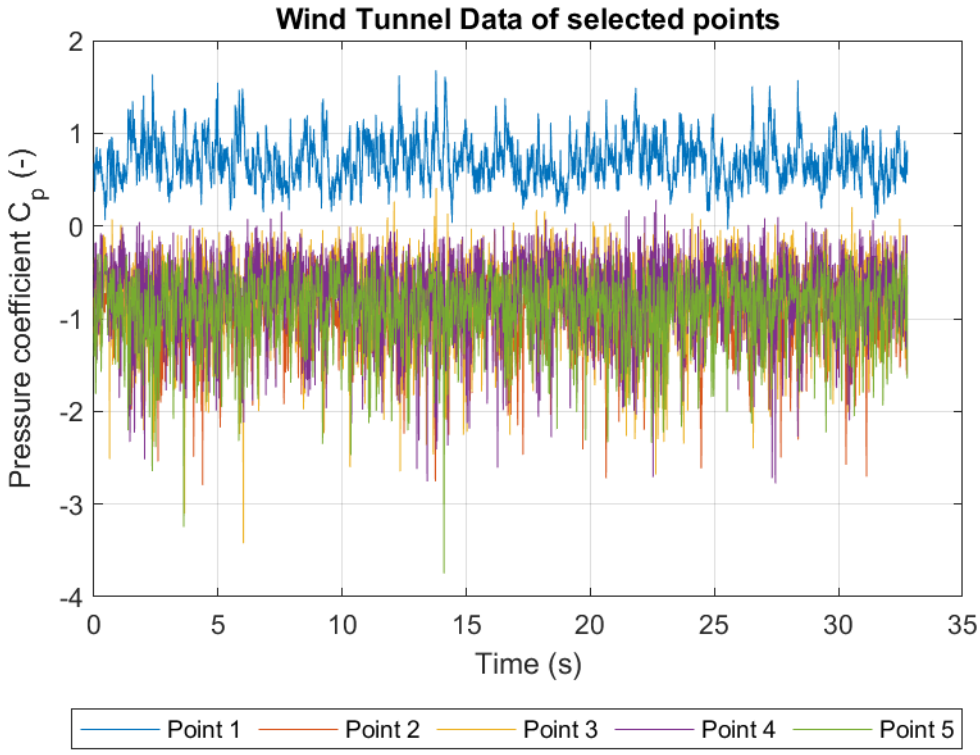

Figure 3.2 Wind tunnel data of selected points for the total simulation time

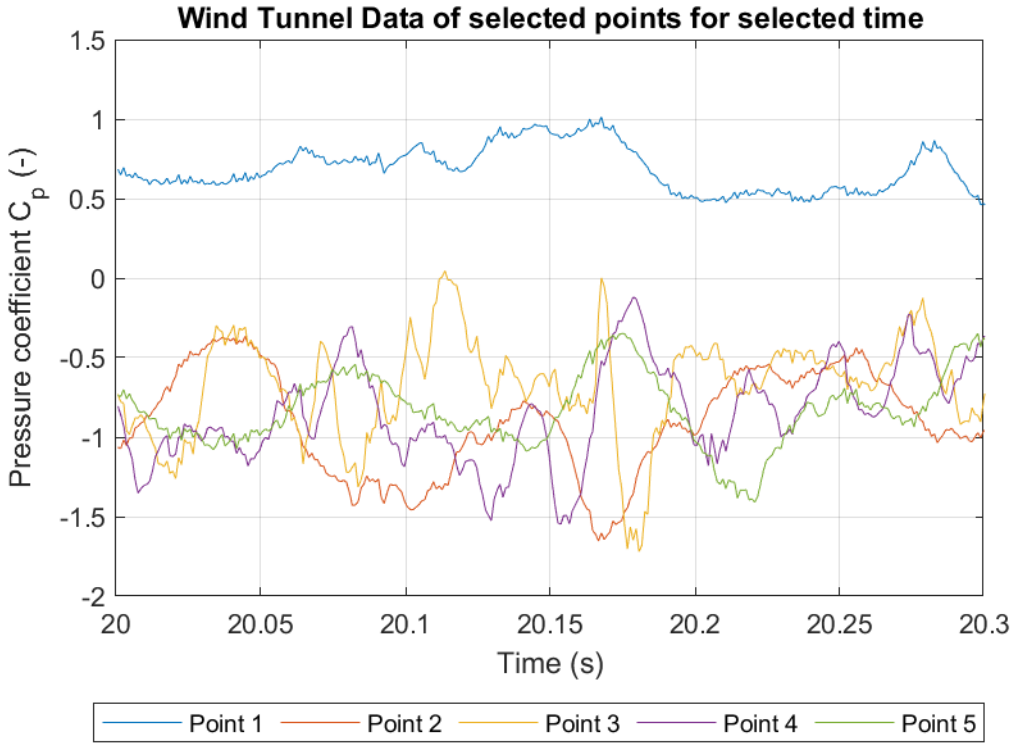

Figure 3.3 Wind tunnel data for a selected time of 0.3 seconds, starting from 20 seconds

The data in Figure 3.3 shows a relatively constant value of roughly 0.7 for Point 1. Since Point 1 is located in the centre of the loaded area, this value is expected to be close to constant. In contrast to Point 1, the pressure coefficients are likely varying over time. Due to the vorticity, it is anticipated that Point 2 and Point 3, located on the right side, show a similar pattern. The

same holds for the points on the left side, Point 4 and Point 5. Due to the vorticity, it is also expected that the left and right sides fluctuate out of phase. This is visible in the data with a period of roughly 0.1 seconds. However, it can also be seen that lots of smaller fluctuations are present. These fluctuations are not on a regular time interval, which would be expected. A reason for this is partly found in the ground effect, which creates a lot of noise. Table 3.2 presents the mean values and the coherent standard deviation of the pressure coefficients on the different points.

Table 3.2 Wind tunnel data, mean value and standard deviation per point

Point	C_{p_μ}	C_{p_σ}
1	0,6997	0,2337
2	-0,8648	0,3317
3	-0,7677	0,3518
4	-0,7503	0,3493
5	-0,8990	0,3461

The wind tunnel data is compared with some basic rules of thumb, presented in Figure 3.4. The most remarkable result is the difference in the quantity of the pressure coefficient of Point 1; this value is underestimated in the experimental results. The rest of the points are in the expected range of reliable results.

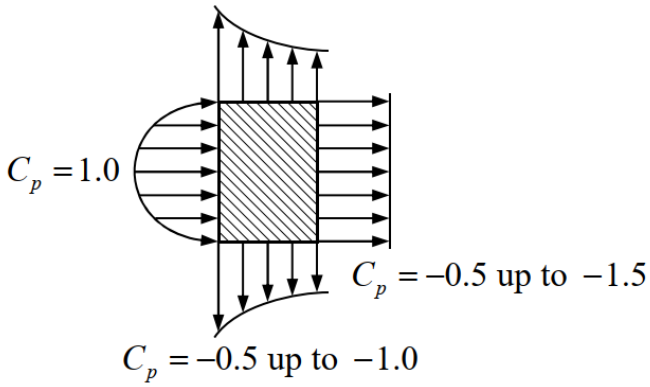

Figure 3.4 Wind pressure coefficients on a block in a uniform flow (Vrouwenvelder, 2004)

The data is transformed to the frequency domain by using a Fast Fourier Transform, and Figure 3.5 presents the results. This confirms the presumption mentioned before; a lot of noise is present in the data.

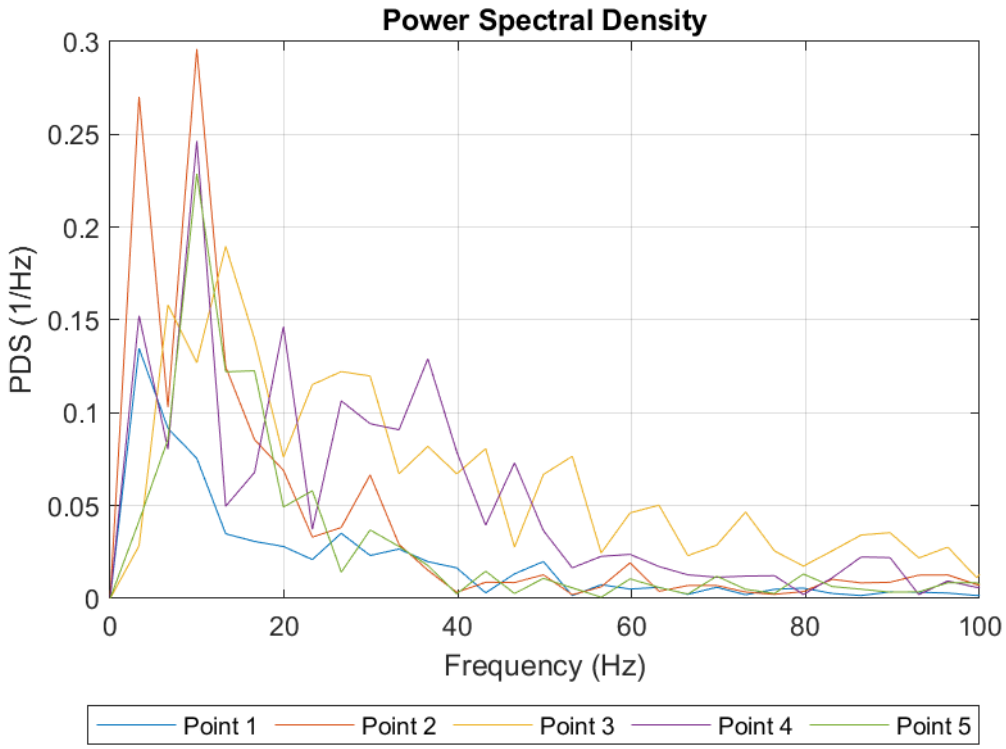

Figure 3.5 Power Spectral Density of the wind tunnel data

Figure 3.5 shows that a lot of energy is present over different frequencies. As shown in Figure 3.3, the closeup of the data visualises a period of around 0.1 seconds. This corresponds with a frequency of 10 Hz, which is visible in the Power Spectral Density graph of Figure 3.5 for Point 2, Point 4 and Point 5.

3.2 CFD simulations

Several CFD simulations are executed to reproduce the results of the wind tunnel data of the Tokyo Polytechnic University, as shown in the previous paragraph. The simulations are performed using Star CCM+ by engineering company ABT B.V. Comparable input to the wind tunnel test is provided to the company to reproduce the wind tunnel data.

Inlet conditions, computational domain and boundary conditions

The geometry of the simulated situation is similar to the reference wind tunnel data. The turbulence intensity is 0.20, and the reference wind velocity is 11.23 m/s on a height of 0.25 meter. Figure 3.6 and Figure 3.7 show a schematic overview.

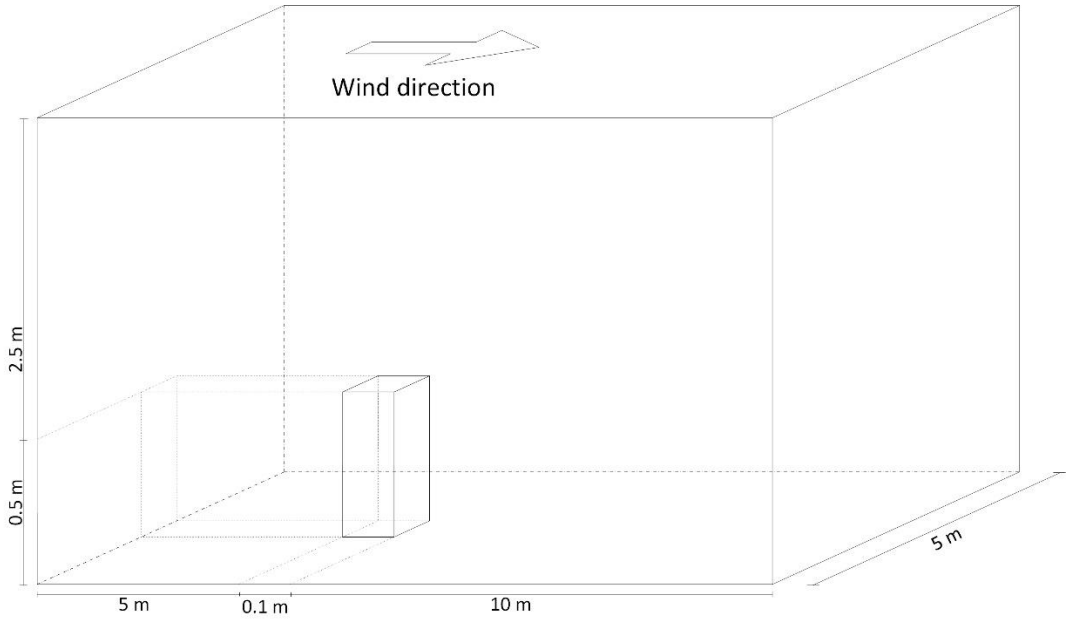

Figure 3.6 Overview of the simulation setup

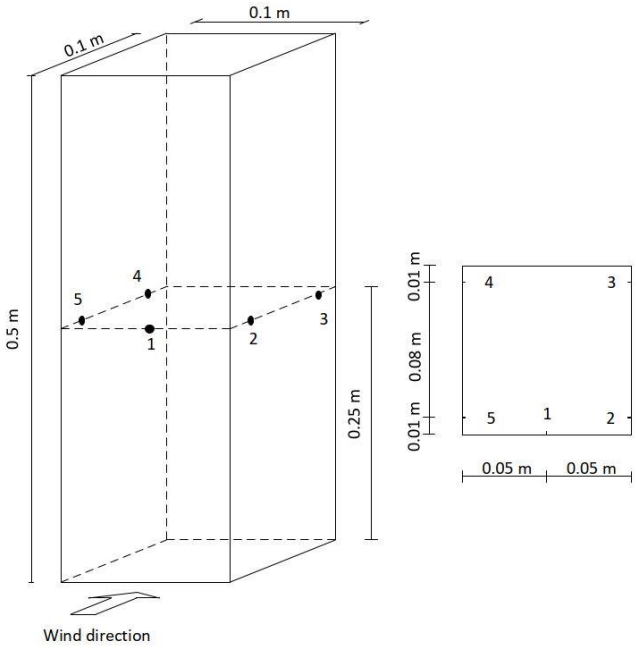

Figure 3.7. Overview of the locations of pressure taps for the CFD simulation of the reference block

The simulations are performed using Star CCM+, a commercial Computation Fluid Dynamics simulation software developed by Siemens. The computational domain has a length of 15,1 meters, a width of 5 meters and a height of 3 meters, and these dimensions are taken according to practical guidelines of CFD simulations(Tu, Yeoh, & Liu, 2018). The dimensions of the model are 0.1 x 0.1 x 0.5 meters. Data points are programmed at the height of 0.25 meters on the locations, as shown in Figure 3.7. A mesh refinement improves the accuracy of the results by using smaller volume cells at critical locations. A total of $1.5 \cdot 10^6$ volume cells define the whole domain, and the mesh is not adapting over time. More than 200 faces of volume cells represent the extracted data on the area with a diameter of 1 mm.

A velocity inlet boundary defines the entrance. Both vertical walls parallel to the wind flow are slip boundaries, which means that the velocity's normal component is equal to zero. On the top of the computational domain is a symmetry boundary specified to enforce a parallel flow. The ground has a no-slip boundary condition, and the wind velocity here is equal to zero. The outlet is defined as a pressure outlet. The freestream fluid density ρ_∞ is taken as $1.18 \frac{kg}{m^3}$ and the dynamic viscosity is $1.85 \cdot 10^{-5}\ Pa \cdot s$.

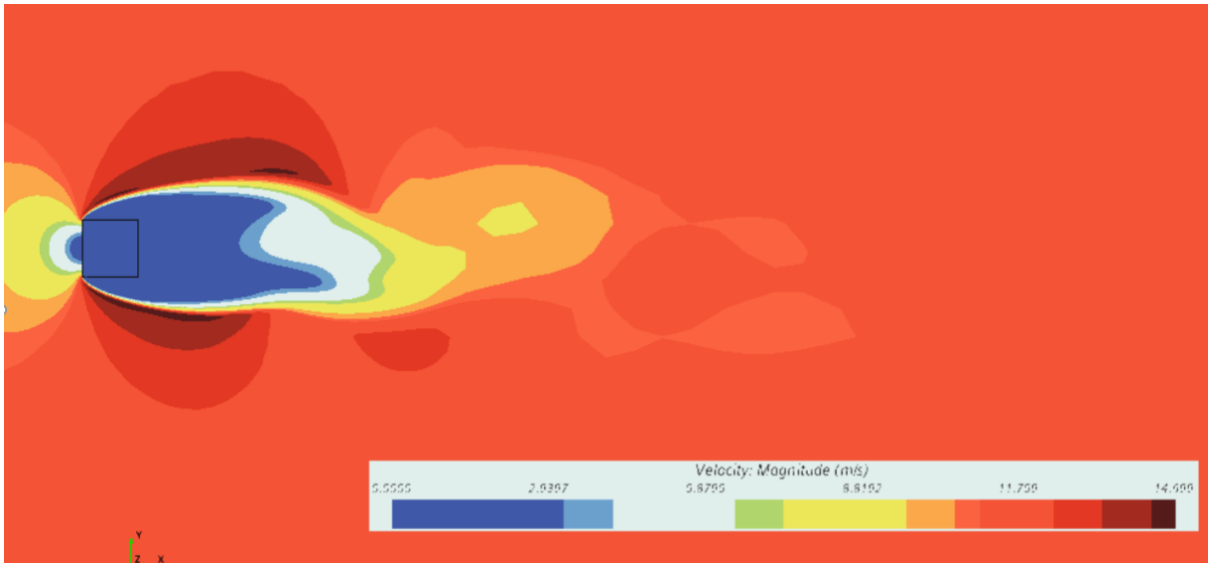

Figure 3.8 Overview of velocities during the simulation of the reference structure

Results

After the refinements of the simulations the following results are obtained: based on a time step of 1^{-4} seconds and with 20 inner iterations a stabilized solution is found, see Figure 3.9. Only the converged data is of importance to obtain relevant results for the frequency domain. Figure 3.10 shows the converged data for a time of 0.3 seconds, starting at 2 seconds.

Table 3.3 shows the numerical values of the results.

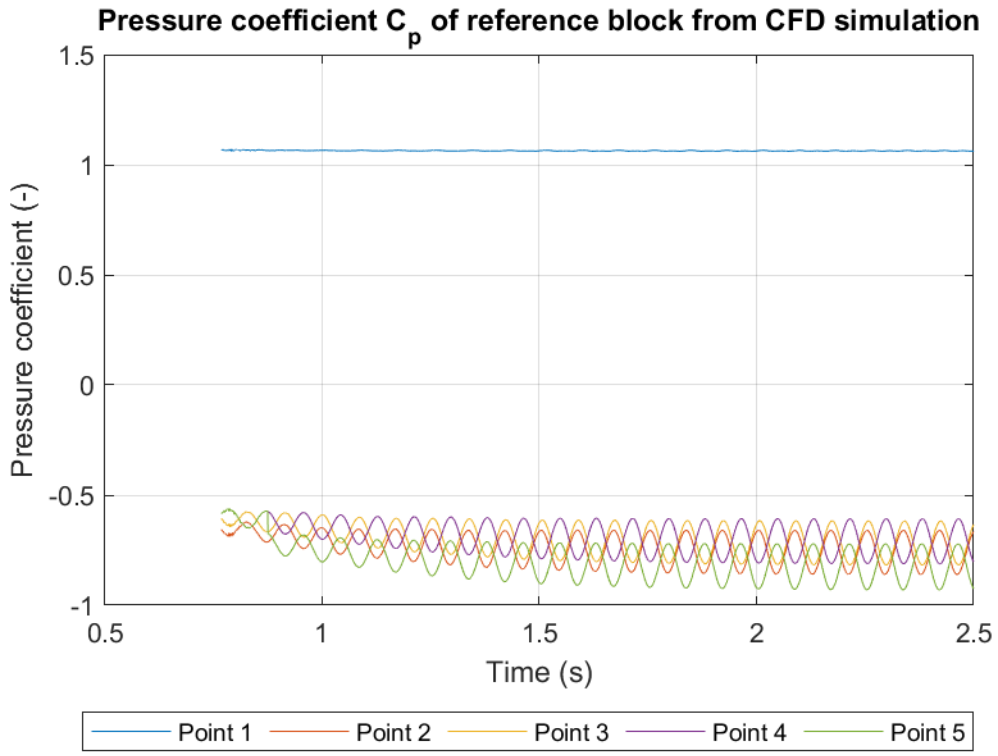

Figure 3.9 CFD results of simulation in the time domain

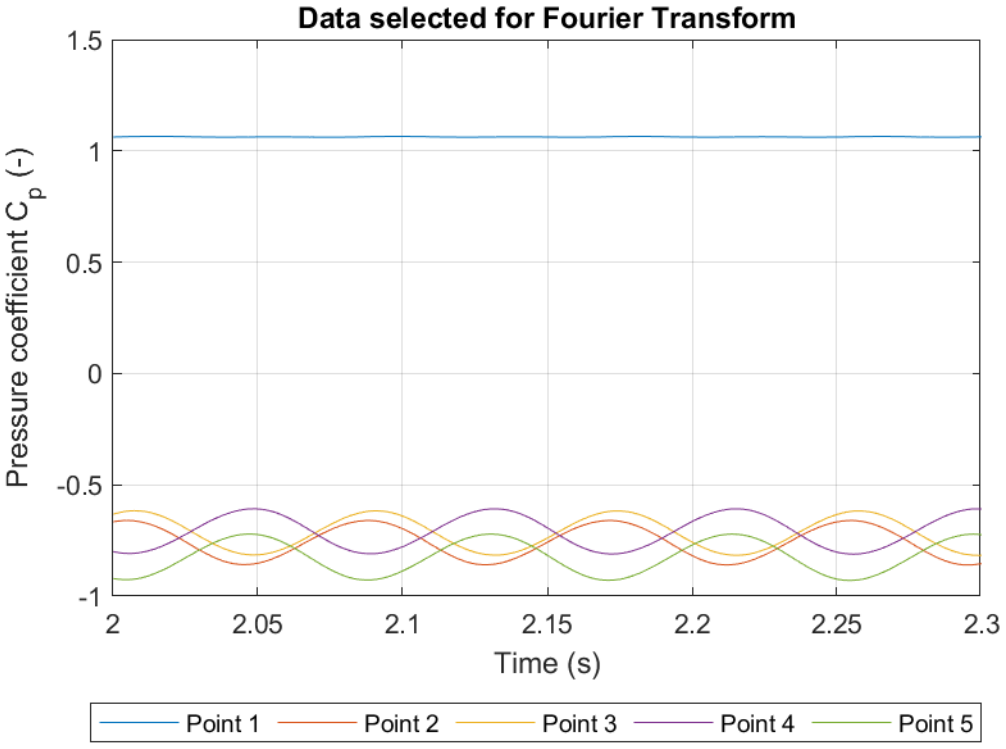

Figure 3.10 Converged data selected for Fourier Transform

Table 3.3 CFD data, mean value and standard deviation per point

Point	C_{p_μ}	C_{p_σ}
1	1,0638	0,0019
2	-0,7269	0,0675
3	-0,6833	0,0687
4	-0,6759	0,0744
5	-0,7664	0,1063

The results in Figure 3.10 show a constant pressure coefficient of Point 1, which confirms the expectations. Point 2 and Point 3 indicate the same oscillating pattern, which is out of phase with the fluctuating way of Point 4 and Point 5. The data gives a clear pattern; only one fluctuation pattern is visible. Further noise of a ground effect is not observable.

The converged data is again transformed into the frequency domain by using the Fast Fourier transform. Figure 3.11 shows the results of the power spectral density.

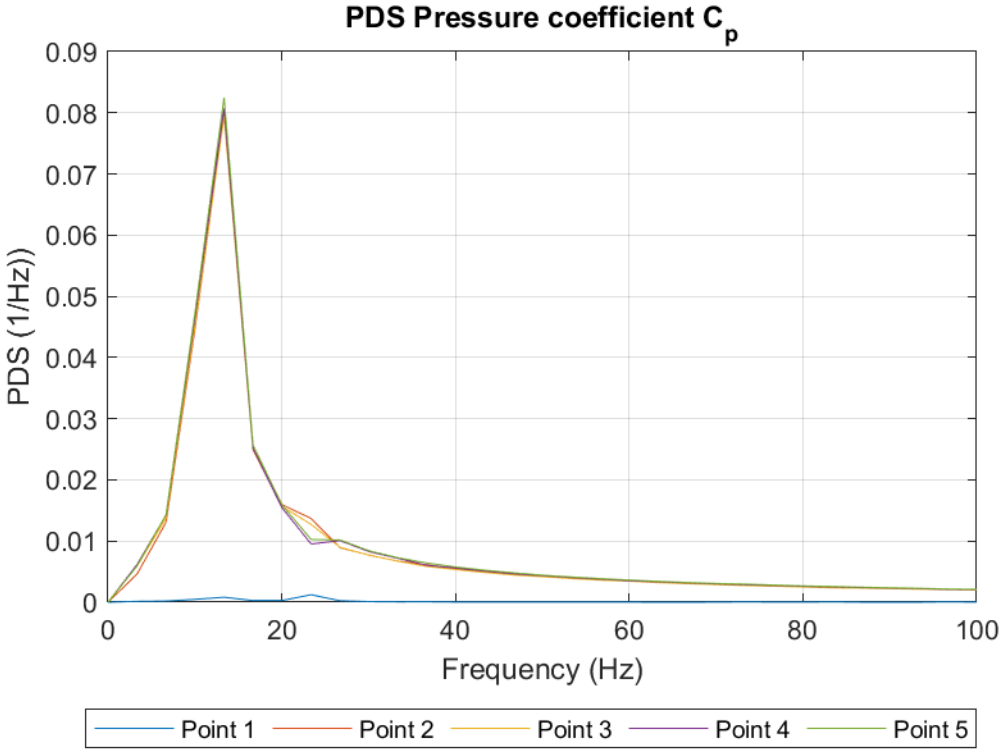

Figure 3.11 CFD results in the frequency domain

A clear peak at 12 Hz is observed in the power spectral density function of the CFD data. Since the data is very clean, no other peaks are relevant. The results of Point 1 show a significantly smaller amplitude in the graph due to the reduced amplitude.

3.3 Validation

The results in the time domain of both the wind tunnel data and the CFD simulations are compared in Figure 3.12 and Table 3.4. The relative difference is calculated in the last column.

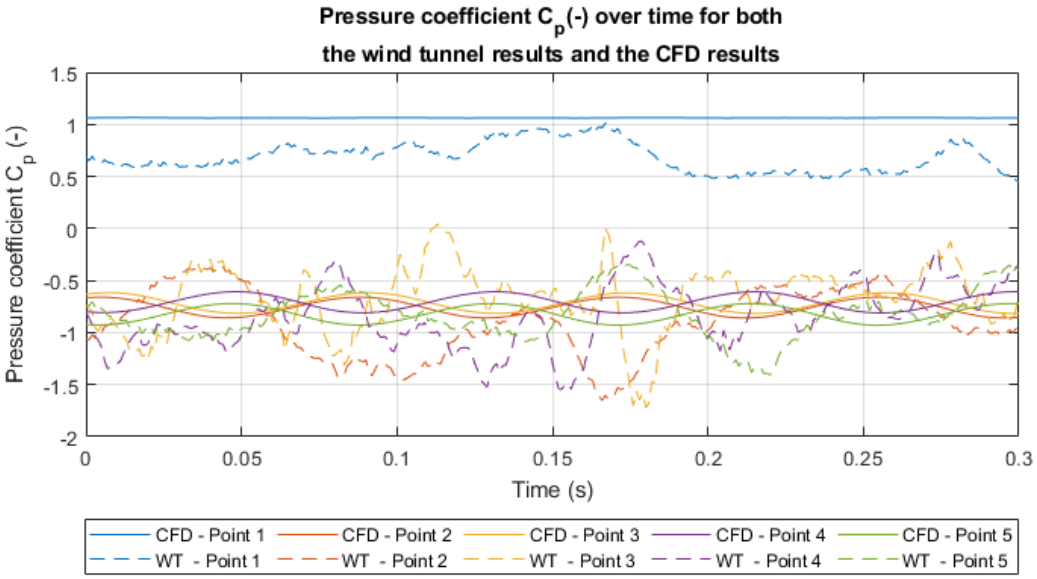

Figure 3.12 Pressure coefficients over time for wind tunnel data and CFD data compared

Table 3.4 Results of the reference block of the wind tunnel data and the CFD simulation summarized

	CFD		Windtunnel		
Point	C_{p_μ}	C_{p_σ}	C_{p_μ}	C_{p_σ}	**Difference in %** $\left(\frac{C_{p_{\mu,CFD}} - C_{p_{\mu,WT}}}{C_{p_{\mu,WT}}} \cdot 100\ \%\right)$
1	1,0638	0,0019	0,6997	0,2337	52,03659
2	-0,7269	0,0675	-0,8648	0,3317	-15,9459
3	-0,6833	0,0687	-0,7677	0,3518	-10,9939
4	-0,6759	0,0744	-0,7503	0,3493	-9,91603
5	-0,7664	0,1063	-0,899	0,3461	-14,7497

From this data, it can be concluded that significant differences are present between the two simulations. The wind tunnel data shows more fluctuations, but in terms of the period the results are comparable. Both simulations show a period around 0.1 seconds, corresponding with a frequency of around 10 Hz. The wind tunnel data shows however more fluctuations and more irregularity. More differences in the irregularity of the values of the pressure coefficients are visible. Especially the mean pressure coefficient value of Point 1 of the CFD simulation looks remarkable, a difference of more than 50 percent is present. For Point 2 till Point 5 differences of 10-15 percent are present, a constant underprediction in the wind tunnel data is observed.

The standard deviation of the pressure coefficient represents the extent of fluctuations in the data. For Point 1 the standard deviations of the wind tunnel and the CFD differ more than a factor of 100, which is highly unlikely to be true. For the other points, the difference is less than a factor of 5. The CFD simulations show immaculate data with a constant lower

fluctuation level of the signal. The wind tunnel data show a significant standard deviation in the result, with a non-constant time lapse.

The results in the frequency domain are also showing significant differences. In the wind tunnel data are no clear peaks observed for any of the points; the data looks random distributed over the different frequencies. The CFD data only show one peak that is clearly visible on 12 Hz. The value of 12 Hz can be checked with the Strouhal number. The Strouhal number describes the oscillating flow mechanism and is defined in Equation (3.2).

$$Sr = \frac{f \cdot L}{v} \tag{3.2}$$

Sr, f, L, and v represent the Strouhal number, the frequency of the vortex shedding, the characteristic length and the flow velocity respectively. The characteristic length is equal to the diameter of 0.14 meter, and the flow velocity is 11.23 m/s. The Strouhal number for square cylindrical shapes lies between 0.15 and 0.2 (Steggel, 1998), resulting in a frequency between 12 Hz and 16 Hz. The results show a clear peak at 12 Hz, which agrees with this basic check based on the Strouhal number.

The differences can be found in several explanations. First of all, the wind tunnel data is normally assumed to be trustworthily, but this data shows a substantial unpredictability. A reason for this could be found in the ground effect. In a wind tunnel usually square blocks are placed between the inlet boundary and the model of interest, these blocks represent the ground roughness. For this data a model with a height of 0.5 meters is used, where data extracted is on a height of 0.25 meters. The ground effect can be dominant on this height, which results in a noisy signal. The dominant period in the CFD simulation is comparable with one of the main periods of the wind tunnel results.

For further studies it is recommended to use other wind tunnel data and to continue improving the CFD simulations until similar results are obtained. For the purpose of this thesis no other simulations were executed.

4. Case study

A geometrically simple high rise structure is used as a case study for the calculations. The dimensions of this structure are 200 meters in height and 40 meters in width. The first natural frequency is 0.2 Hz, and a wind velocity with a return period of 25 m/s is chosen, this is a standard reference for Western Europe. The roughness length is taken as 0.1 meters. The building's mass is 7500 kg/m^2 per unit loaded area in the considered direction and taken constantly over the height. Only the movements in de along-direction of the wind are considered. The structural damping is 1% of the critical damping. Equation (4.1) computes the Reynolds number.

$$Re = \frac{v \cdot d}{\nu} = \frac{25 \cdot 40}{1.55 \cdot 10^{-5}} = 6.5 \cdot 10^{7} \tag{4.1}$$

Here v is the the wind velocity, d the diameter of the model and ν the dynamic viscosity of $1.55 \cdot 10^{-5}\ Pa \cdot s$. The result is a Reynolds number of $6.5 \cdot 10^{7}$, which is highly turbulent.

The calculations are performed using the spectral approach and are compared with the two procedures of the Eurocode to calculate the structural factor $c_s c_d$. Afterwards, the loads and the load spectrum are compared to the CFD simulation provided by engineering company ABT B.V.

4.1 Wind calculations by the spectral approach

The wind profile is obtained using the procedure given in Chapter 2.3. Figure 4.1 shows the incoming wind profile characteristics. Only the first eigenmode Φ_I is taken into account, Equation (4.2) describes this linear eigenmode.

$$\Phi_I = \frac{z}{h} \tag{4.2}$$

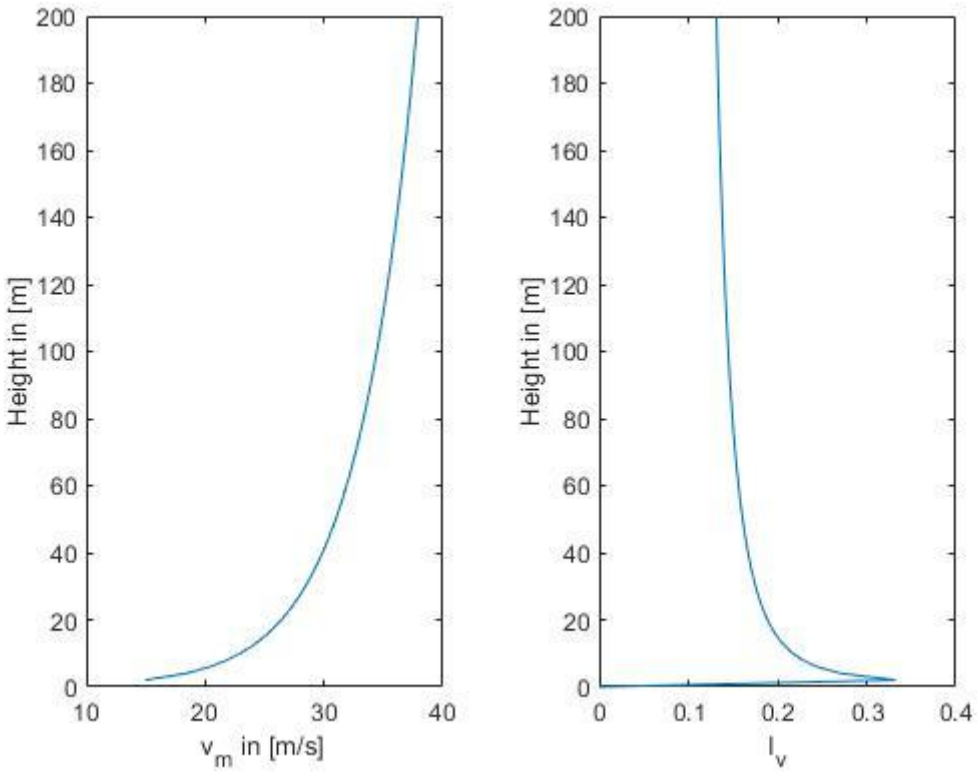

Figure 4.1 Left: Wind velocity profile characteristics over height. Right: Turbulence intensity profile over height.

The fourth integral of the coherence function is needed to calculate the aerodynamic admittance, see Equation (4.3) and Equation (4.4).

$$coh_{v_k v_l}(n) = e^{\frac{-2\,n}{v_m(z_k)+v_m(z_l)}\sqrt{C_z^2(z_k-z_l)^2+C_y^2(y_k-y_l)^2}} \tag{4.3}$$

$$X_{\Phi_i}^2(n) = \frac{1}{A^2}\int_h\int_h\int_b\int_b \frac{v_{m,k}}{v_{m,z_s}}\frac{v_{m,l}}{v_{m,z_s}}\,\Phi_i(y_k,z_k)\,\Phi_i(y_l,z_l)\,coh_{v_k v_l}(n)\,dy_k dy_l dz_k dz_l \tag{4.4}$$

Equation (4.3) and Equation (4.4) could not be solved analytically due to the complexity of the function and computational limitation. Two different methods are used to approximate these functions. The first method is an approximation with a Monte Carlo integration. Multiple combinations of random numbers between the boundaries of the integral are generated and the value of the $X^2_{\Phi_i}(n)$ is calculated by computing the mean of the all generated values. This method depends highly on the number of generated random values and can get unstable when too many random samples are used.

The second method is a discretization of the surface of the façade. The façade is divided into smaller surface areas, and results are calculated per area. The sum of all those components provides the result. The size of the surfaces highly determine the accuracy of the solution. Smaller areas result in more accuracy but also cost more computational time. In the end, a solution was found making a mesh of 2.5 x 2.5 meter. Smaller mesh sizes did not result in better results.

Figure 4.2 presents the result of both approximations. Since the Monte Carlo approximation appeared to be less stable, the discretized approximation is used in further calculations. A more detailed overview of these calculations is given in Appendix A- Monte Carlo Simulation

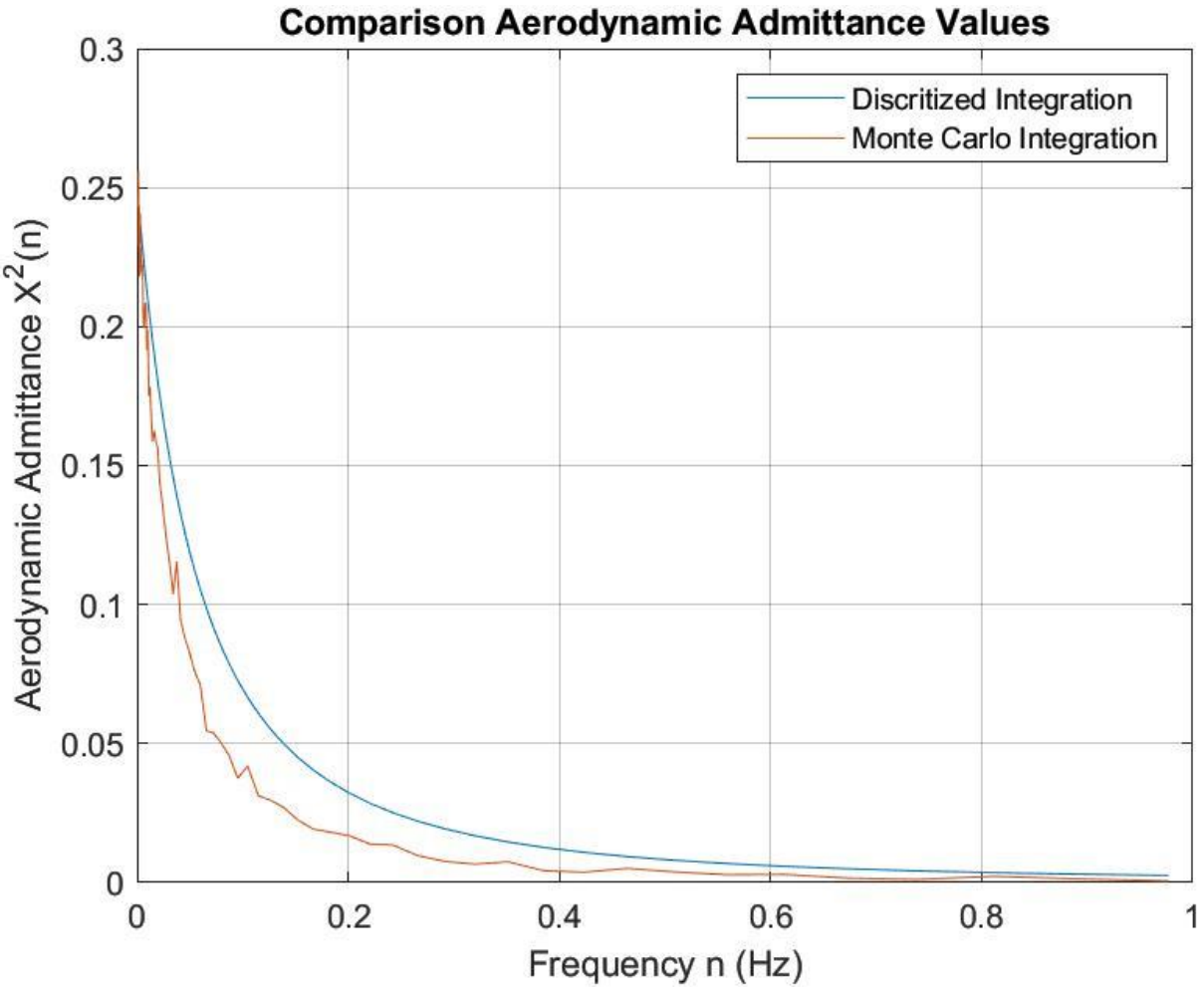

Figure 4.2. Comparison of $X^2(n)$ approximated by different methods

To validate the calculations, a comparison between the structural factor $c_s c_d$ of the theory and procedure 1 and 2 of the Eurocode is made. Table 4.1 present the results.

Table 4.1. Comparison of the values of the structural factor

	Theory	**Procedure 1 Eurocode**	**Procedure 2 Eurocode**
Structural factor $c_s c_d$ calculated	1,08	1,03	1,07
Structural factor $c_s c_d$ from (Steenbergen et al., 2012a)	1,09	1,03	1,07

A difference can be observed in the theoretical value of the structural factor. This difference can be found in the accuracy when approximating these integrals. The discretization for the aerodynamic admittance and the integral taken afterwards are here the main parameters. For example, to calculate the Γ, as shown in Equation (2.23) assumptions are made regarding the range of frequency n. The range of the frequency is taken in the logarithmic space and from 10^{-3} to 10^{1} Hz. Changing the lower limit to 10^{-6} Hz changes the structural factor of the Matlab calculations to 1.09. However, due to the computational time this calculation requires, it is chosen to limit the frequency range from 10^{-3} to 10 Hz.

Figure 4.3 shows the summarized results of the spectral approach. A more detailed overview of these calculations is given in Appendix B – Spectral Approach.

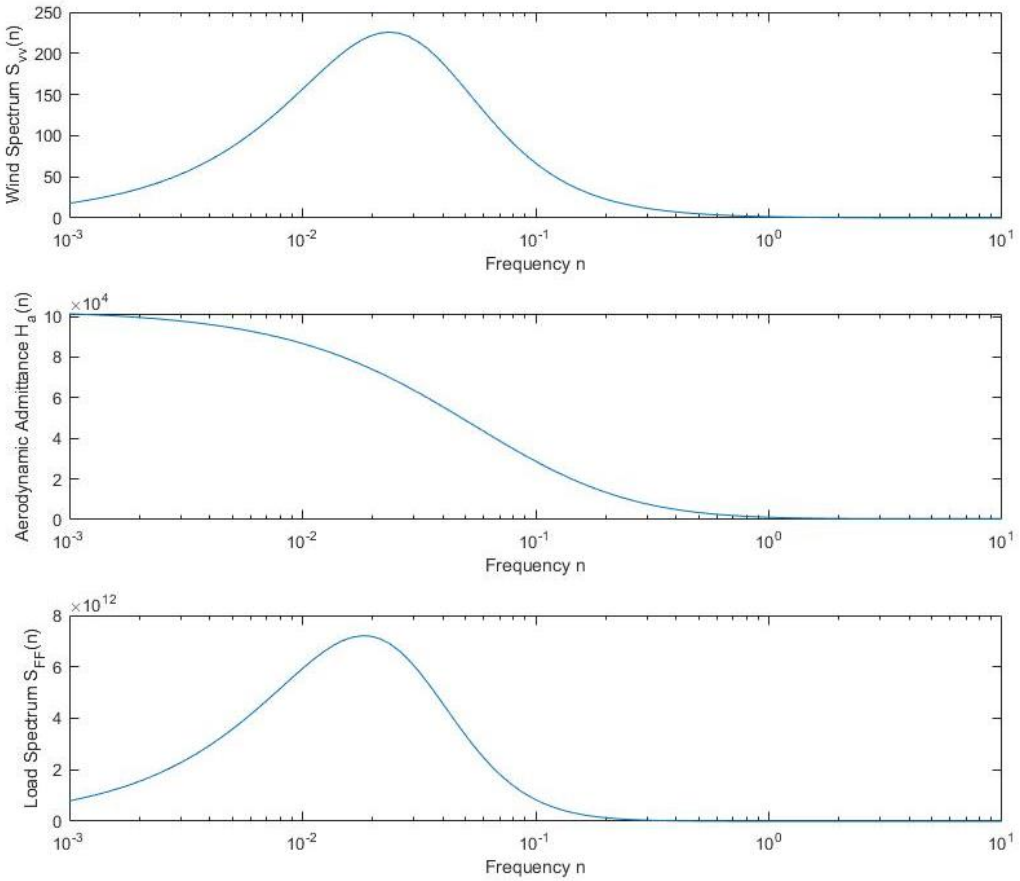

Figure 4.3. Wind Spectrum, Aerodynamic Admittance and Load Spectrum for case study

For comparison with the CFD simulations results, the pressure at the height of 150 meters is of importance. The pressure on this height has a mean value of 781 Pa and a standard deviation of 279 Pa. The peak velocity pressure is added to the table according to Equation (4.5).

$$q_p = q_\mu + k_p \cdot q_\sigma \tag{4.5}$$

Where $\hat{q}$ is the peak velocity pressure, μ the mean value of pressure, g the peak factor of 3.5 (Steenbergen et al., 2012b) and σ the standard deviation of the pressure.

Table 4.2 Results of the spectral approach

Point	Mean pressure q_μ (Pa)	Standard Deviation of the pressure q_σ (Pa)	Peak pressure q_p (Pa)
P1 + B1	781	279	1611
P2 + B2	781	279	1611
P3 + B3	781	279	1611
P4 + B4	781	279	1611

4.2 CFD simulations

Multiple CFD simulations are executed in collaboration with engineering company ABT B.V. To limit the computational time, keep file sizes manageable and limit the coherent costs, only pressure measurements are extracted at the height of 150 m. The first simulation is semi two-dimensional, which means that a thick imaginary strip is taken in the three-dimensional space. The wind velocity is only accurately simulated in the domain covered by this strip and bounded with slip boundaries; this simulation is called two-dimensional from now on. The stored data on the surface is averaged over 10 x 10 meters, so in the 2D simulation is no development over height visible in the results. Afterwards, a three-dimensional simulation is performed where the wind velocity in the whole domain of the setup is simulated.

Inlet conditions

The inlet condition is defined with an incoming wind velocity profile similar to the spectral approach. The turbulence intensity is characterized by the turbulent kinetic energy k in J/kg. The turbulence kinetic energy is defined as the half of the sum of the standard deviations of the velocities in the three dimensions, as shown in Equation (4.6).

$$k = \frac{1}{2}\left(\sigma_{v,x}^2 + \sigma_{v,y}^2 + \sigma_{v,z}^2\right) \tag{4.6}$$

The spectral approach uses a fixed turbulence intensity profile varying over height, as shown in Figure 4.1. The CFD simulations approximate the turbulence over the domain by an adaption criterion function. This function calculates the turbulent kinetic energy for all cells. Only the range of the turbulence kinetic input is defined, this range is between 50 and 2160 J/kg.

As mentioned before, results are only extracted at a height of 150 meters. The obtained pressure values are the mean value for an area of 10 x 10 meters on the façade. The locations and numbering are shown in Figure 4.4, where P1 till P4 are located on the windward side and B1 till B4 are located on the leeward side. The velocity- and the turbulence intensity profile

are described according to the procedure of the Eurocode. The basic wind speed is $25\,m/s$ and the roughness height as $0.1\,m$. This results in the same wind velocity- and turbulence intensity profile, as shown in Figure 4.1.

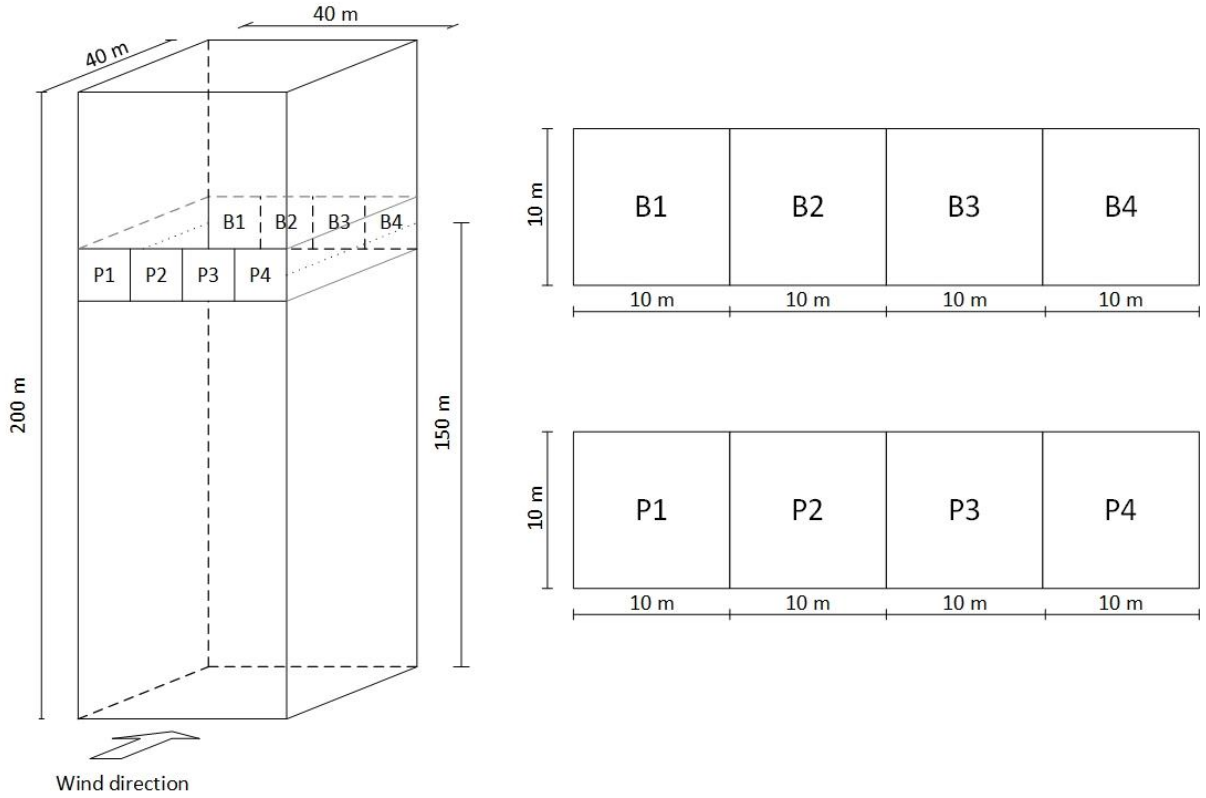

Figure 4.4. Left: Schematic overview of the wind on the building, including dimensions and wind direction. Right: an overview of the names and coherent areas of the pressure measurements on the façade.

The boundary conditions are imposed artificially since the computational domain has to be finite. Therefore the area around the building is constrained by boundaries. These boundaries and their dimensions are designed by using rules of thumb for CFD simulations. The domain is shown in Figure 4.5.

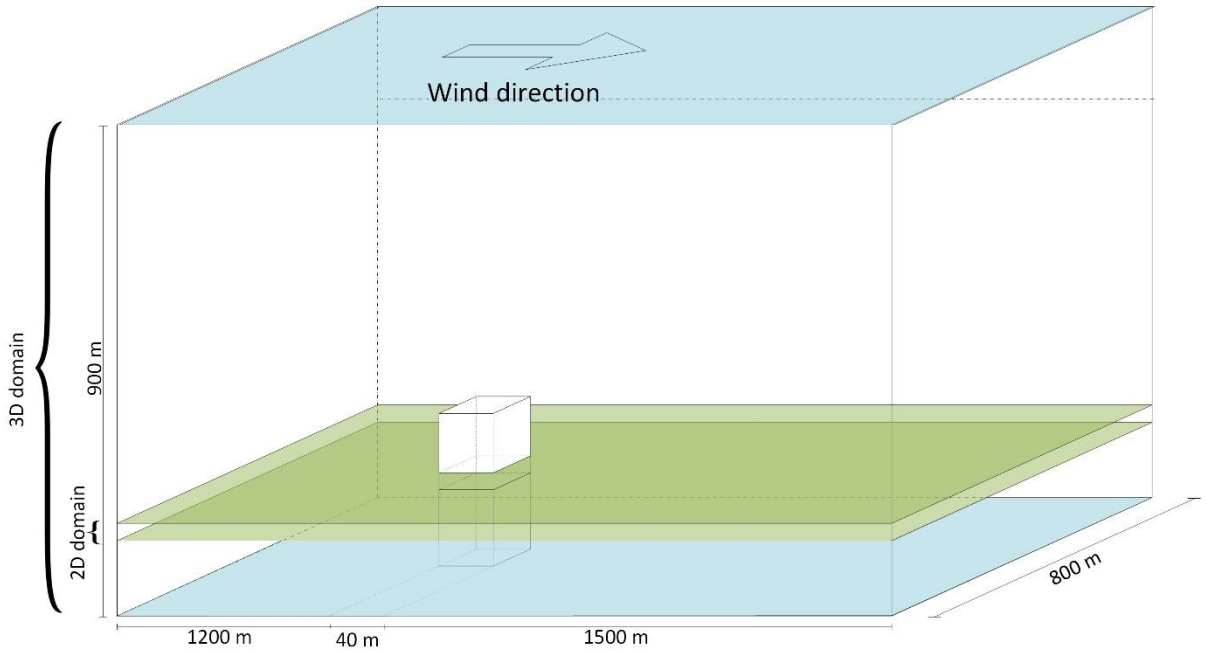

Figure 4.5. Setup CFD simulations, including dimensions of the domain

The boundaries have to be appropriately defined to produce realistic numerical results. The velocity defines the inlet boundary- and turbulence intensity profile; the outlet boundary is a free pressure outlet. The side walls are defined with slip boundaries, the flow velocity is only present parallel to boundary, and no normal velocity components are present. The floor's effect is represented on the bottom surface with a no-slip boundary, and the top of the simulation is defined with a symmetry boundary condition. The top surface is considered high enough not to influence the relevant elevation level of interest. (Rusdin, 2017). More than $5.5 \cdot 10^6$ volume cells characterize the domain. An adaptive mesh is used to improve the mesh density over time. The adaptive mesh results in roughly 400 volume cell faces for P1 and P4, where the results of P2 and P3 are obtained from the average of 225 volume cell faces.

2D simulation

The two-dimensional simulations are performed first. The simulations are run until constant oscillation patterns are observed. The pressure over time per pressure point is presented in Figure 4.6. Only pressure points P1 till P4 were logged in this simulation, the data on the pressure points on the backside B1 till B4 was not stored while running the simulation.

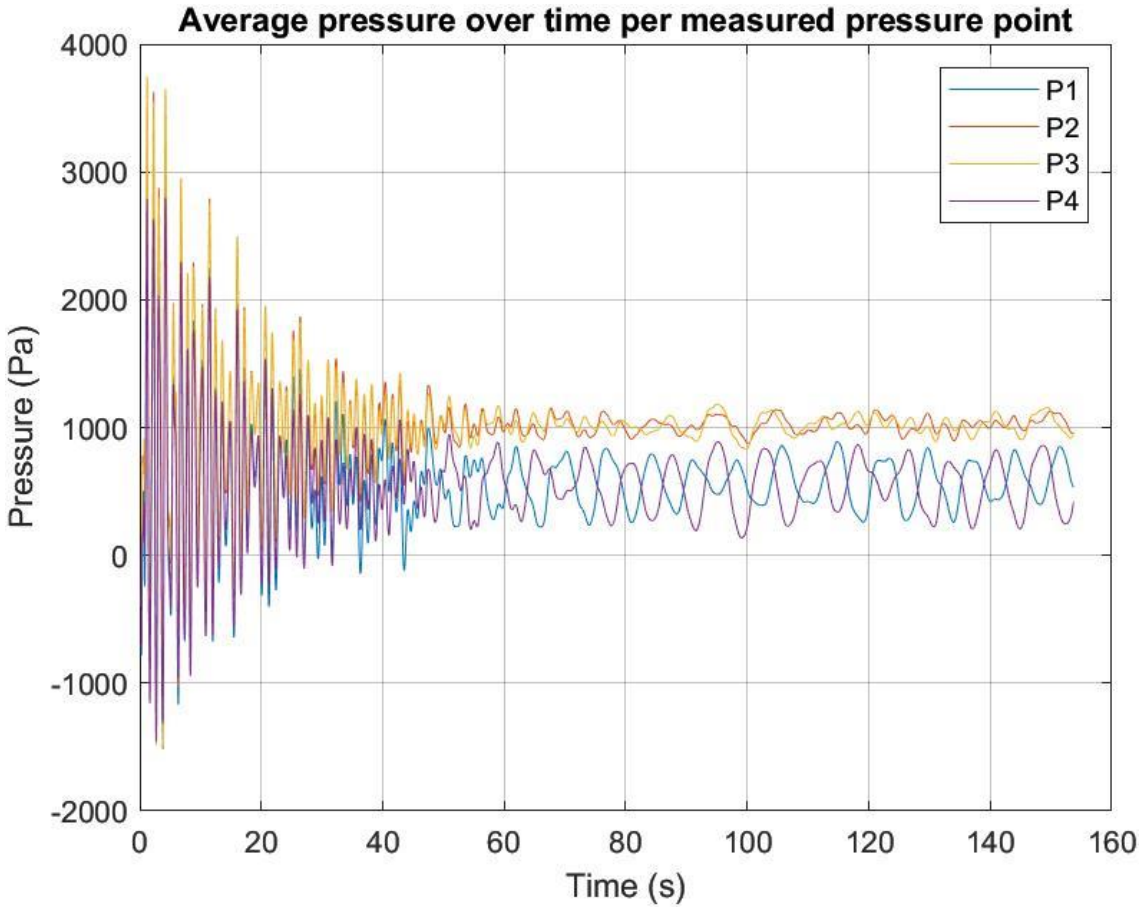

Figure 4.6 Pressure over time per pressure point for the 2D simulation

The results show a constant oscillating pattern from 60 seconds onwards. A converting turbulent pattern can be seen in the first 60 seconds. This can be explained due to the stabilization of the inlet conditions when passing the domain. This effect is often observed in CFD simulations, and the main part of interest for these results is the stabilized pattern from 60 seconds onwards. To illustrate the convergence to a steady-state solution, the pressure values of P1 are analysed in Figure 4.7. The local maxima and local minima are presented with a trendline through these peaks. The trendline ends in two parallel horizontal lines, which means that the pressure signal converged to its steady state. Similar results are obtained for the other pressure points P2, P3 and P4. When the stabilized pattern is analysed, the converged data is used to extract the results' absolute values in the time domain and the frequency domain. The sourced data for the Fourier transformation is presented in Figure 4.8.

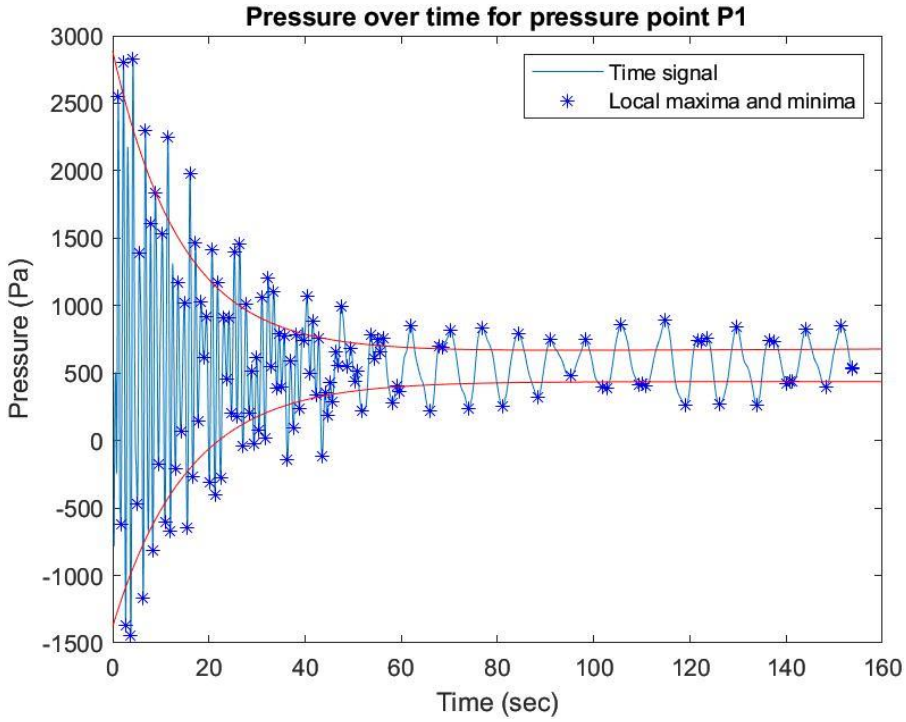

Figure 4.7. Pressure over time for pressure point P1 with local maxima and minima

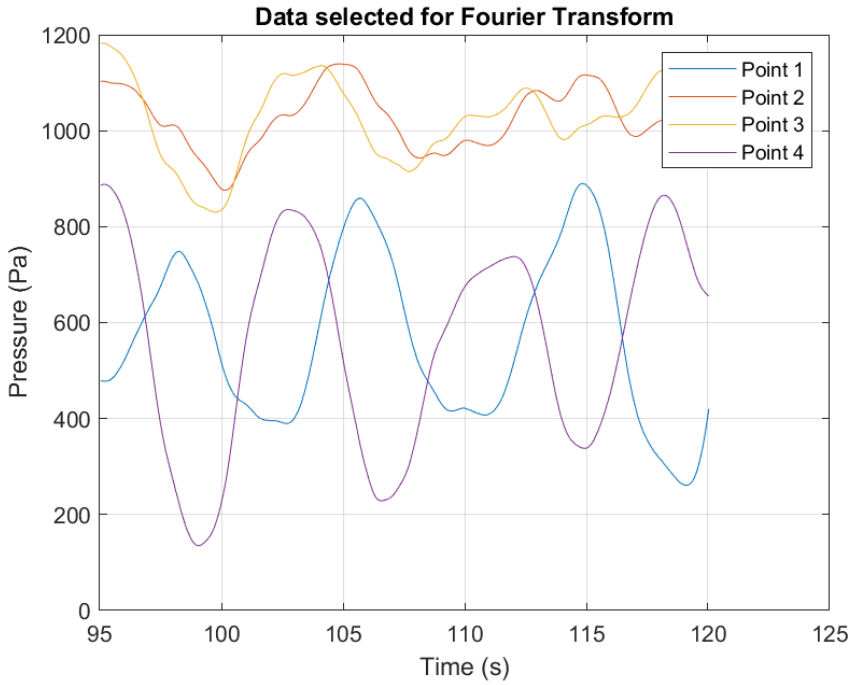

Figure 4.8 Data selected for Fourier transform

These results are presented in Table 4.3. The results show that the values of P1 and P4 are in the same range, the same holds true for P2 and P3. This similarity is expected due to the symmetry of the setup and the measured point on the façade.

Table 4.3 Mean pressure values per pressure point for the 2D simulation

Point	Mean Pressure q_μ (Pa)	Standard deviation of the Pressure q_σ (Pa)
P1	563	173
P2	1022	65
P3	1022	84
P4	560	220

The results presented in Figure 4.7 are stated in the time domain. The Fourier Transform is used to convert the results to the frequency domain. The Power Spectral Density of the pressure describes the power present in the signal as a frequency function.

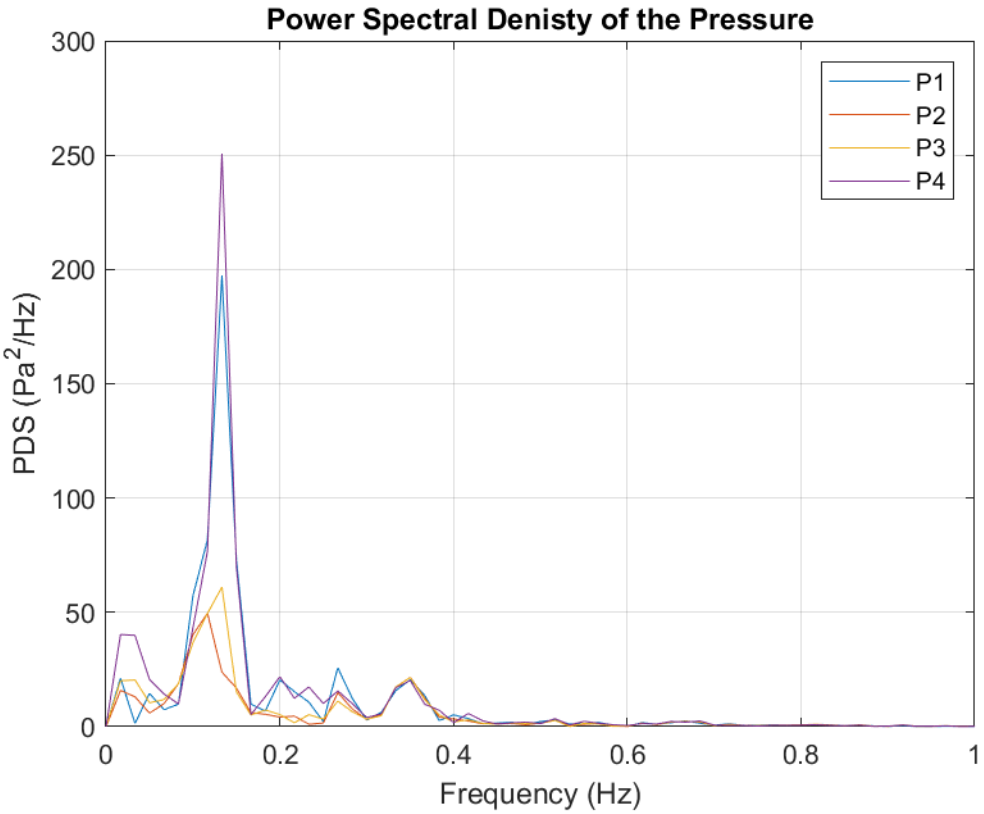

Figure 4.9. Power Density Spectrum for all measured pressure points for a time sample of 95-120 sec

Clear peaks are observed on a frequency of around 0.12 Hz. The height value of the peaks is for outer points P1 and P4 larger compared to the other inner pressure points, and this difference is expected since the outer edges encounter more variance due to the vortices around the structure.

3D simulation

Two three-dimensional simulations were performed as well to check if the results are comparable with the two-dimensional simulation. For the 2D simulation, only a strip of the domain was chosen. In the 3D simulation the whole domain is used to simulate the wind profile. After analysing the first 3D simulation, it was concluded that the results did not capture realistic physics. Therefore, a second 3D simulation was performed. The first 3D simulation contains different initial conditions than the second 3D simulation. Both the results are described in this chapter. The results of both the windward side P1 till P4 and the leeward side B1 till B4 are stored while running the 3D simulations.

The inlet conditions regarding the velocity- and turbulence intensity profile are similar to the semi-2D simulation, but the wind is now developing in three dimensions. This means, for example, that the roughness of the bottom influences the wind profile near the ground. It also means that there now is an interaction between the vertically stacked layers.

Again, the goal is to reach a constant oscillating pattern for pressure over time. It arrests attention that the pressure over time seems to converge to a constant pressure value; this is illustrated in Figure 4.11. The 2D simulation converged to a constant oscillating pattern with an amplitude, and these results converge to a constant without amplitude.

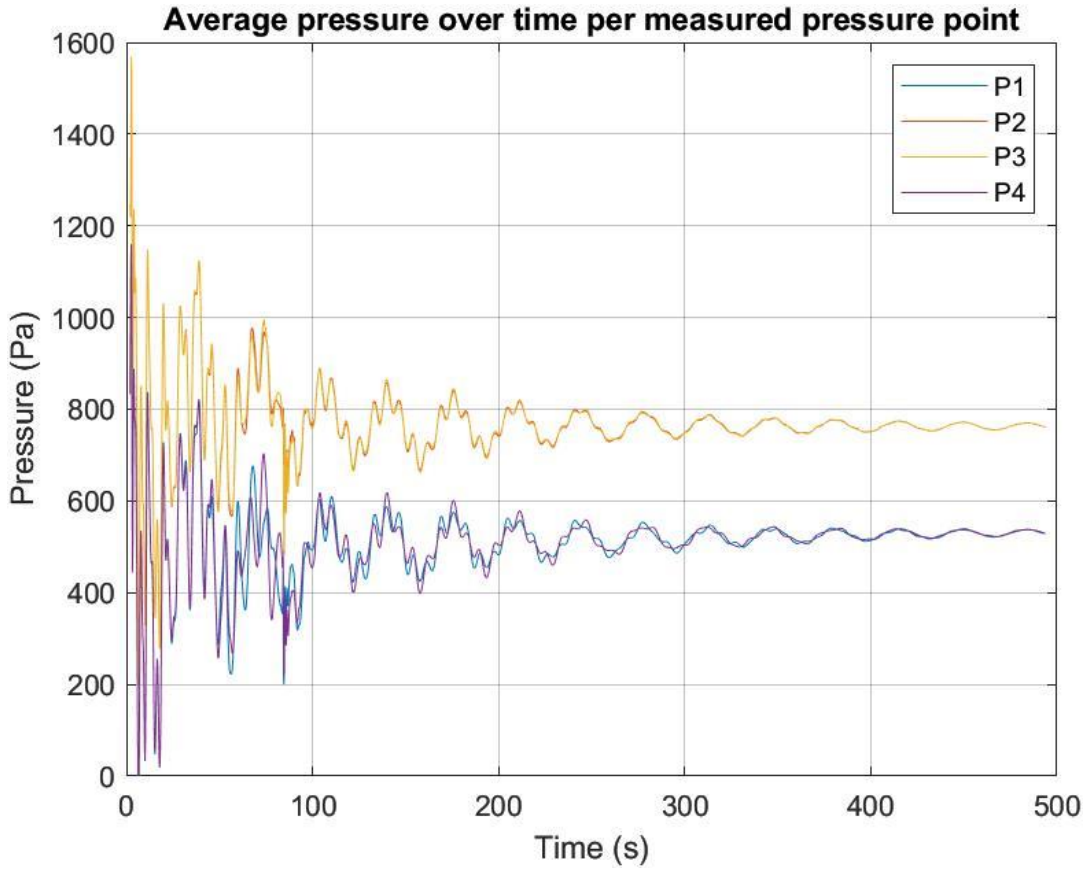

Figure 4.10. Average pressure over time per measured pressure point for the first 3D simulation

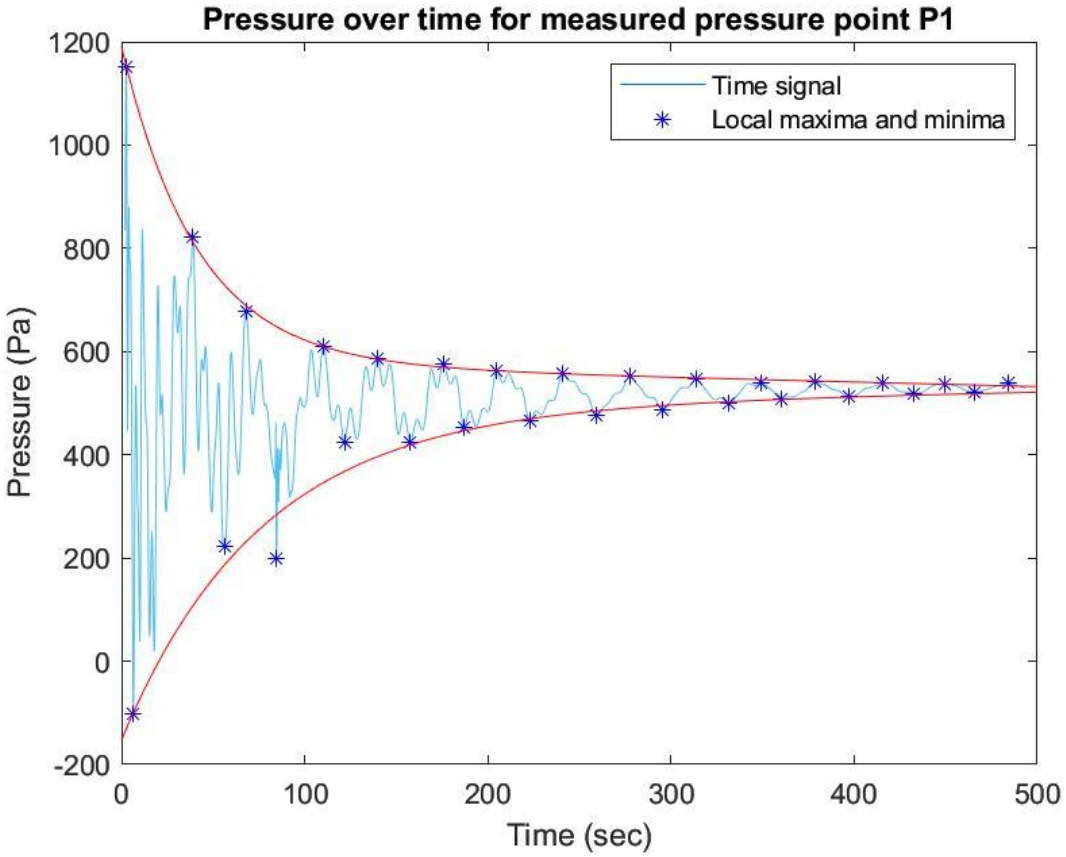

Figure 4.11. Pressure over time for measured pressure point P1

These results were not expected, and a closer look into the simulation process is taken in the simulation process. It turns out that the plot samples of the simulations are not sufficient to capture the relevant physics. A more detailed description of these results can be found in Appendix E – Analysis of first 3D simulation. For the second 3D simulation the plot sample has changed from 20000 to 50000. The results of the second simulation are shown in Figure 4.12. For this simulation, both the windward and the leeward side are taken into account. The results on the windward side are positive pressure values, which is expected. The leeward side results are negative values, which means that a wake is present behind the structure.

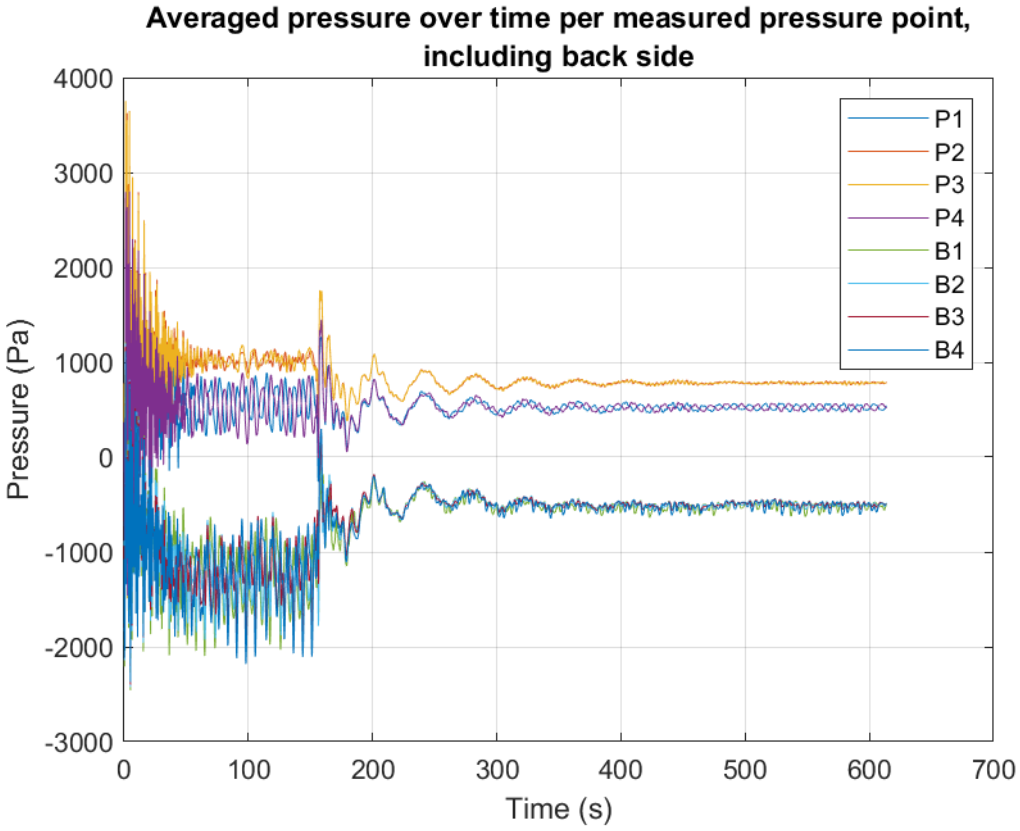

Figure 4.12 Average pressure over time per measured pressure point for the second 3D simulation

The second 3D simulation results require extra explanation, after a time of 160 seconds, there is a different pattern visible then in the first 160 seconds. These results can be seen as the results of two different simulations. The first 160 seconds show the results of the semi-2D simulation. This is done to get proper initial conditions for the actual simulation. When a CFD simulation is performed, the computation domain is divided into different meshing cells. Each cell requires several quantities, such as pressure and temperature. Over time are the quantities developing using difference schemes. The first phase of a simulation is highly converting to a more stable signal, where a realistic balance of the solved Navier Stokes equation quantities is pursued. The results of the semi-2D simulation are used to create initial conditions for the 3D simulation. In this simulation, the pressure converts to a constant oscillating patter from 500 seconds onwards. The remaining oscillation has a period of around 12 seconds. The main oscillation with a period of around 40 seconds, that is observed between ~220 and ~420 seconds slowly fades away. This is the same oscillation that as fading away in the first analysis (Figure 4.11), but then the plot samples did not capture the underlying oscillation with a period of around 12 seconds emerging. An overview of the simulation development over time is shown in Appendix F – Development of the 3D simulation

It is also observed that results of the leeward side, B1 till B4, are significantly lower for the first phase where the initial conditions are determined in the 2D simulation. This can be explained by the wake blockage effect. The top of the structure creates a trailing vortex which disturbs the wind velocity pattern around the building. This principle is illustrated in Figure 4.14, where on the left a situation is sketched where the height is longer than the critical length and on the right, a situation is sketched for the same cylinder but shorter than the critical height. In the

2D simulation, the wake blockage effect is not present. The Kárman vortex is dominant and creates a significant suction behind the structure. When the 2D simulation converts to the 3D simulation, the trailing vortex develops and the suction decreases.

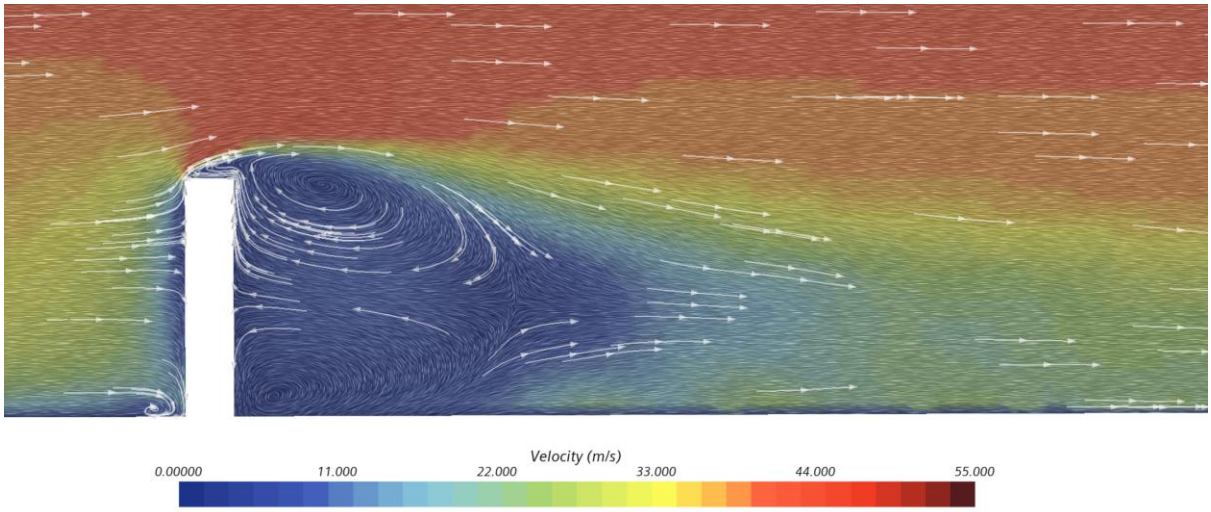

Figure 4.13. Velocity profile around the structure

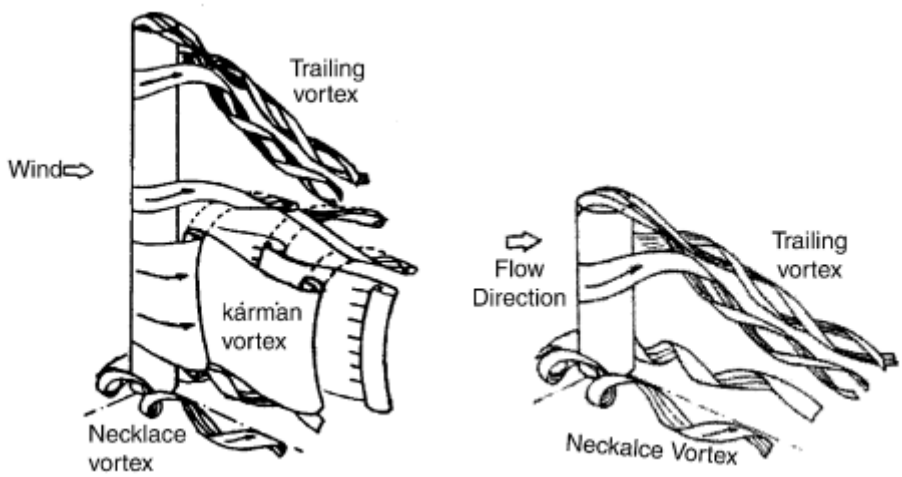

Figure 4.14. Sketches of the flow field around a cylinder of a finite height (Fröhlich & Rodi, 2004)

For further calculations, the front and backside results are combined, resulting in a total pressure in the windward direction per area. The converged pressure results from 500 to 600 seconds, shown in Figure 4.15, are used to obtain the power spectral density and the mean and standard deviation of the results. The power spectral density results are presented in Figure 4.16 and the mean and standard deviation of the wind pressure are shown in Table 4.4.

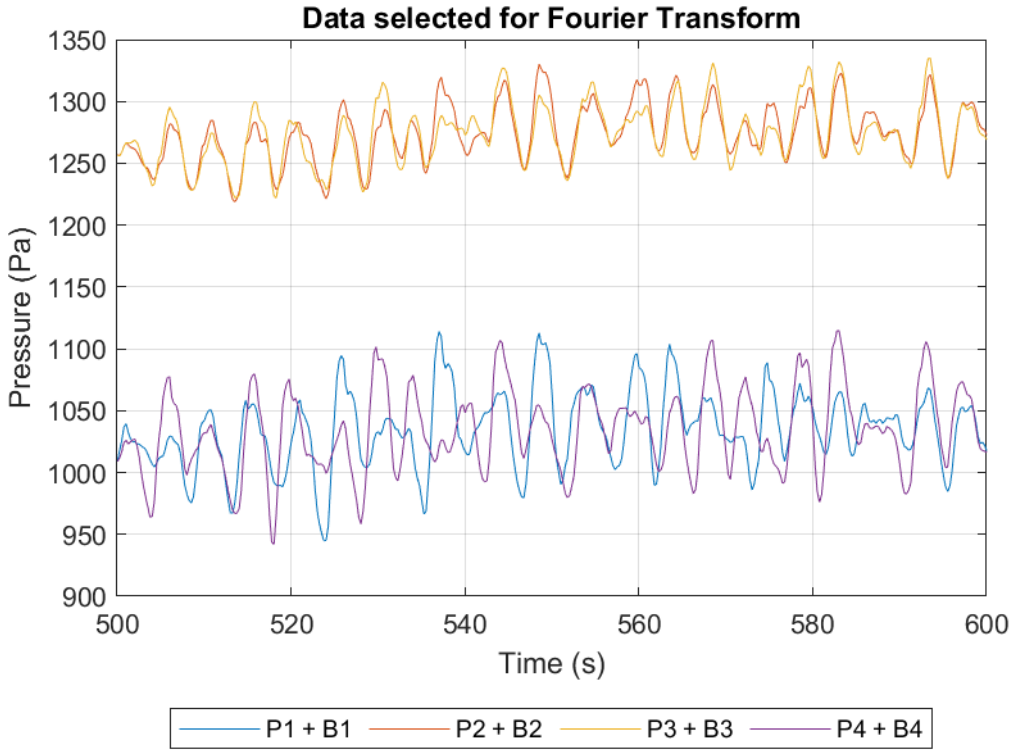

Figure 4.15 Converged data from the second 3D simulation

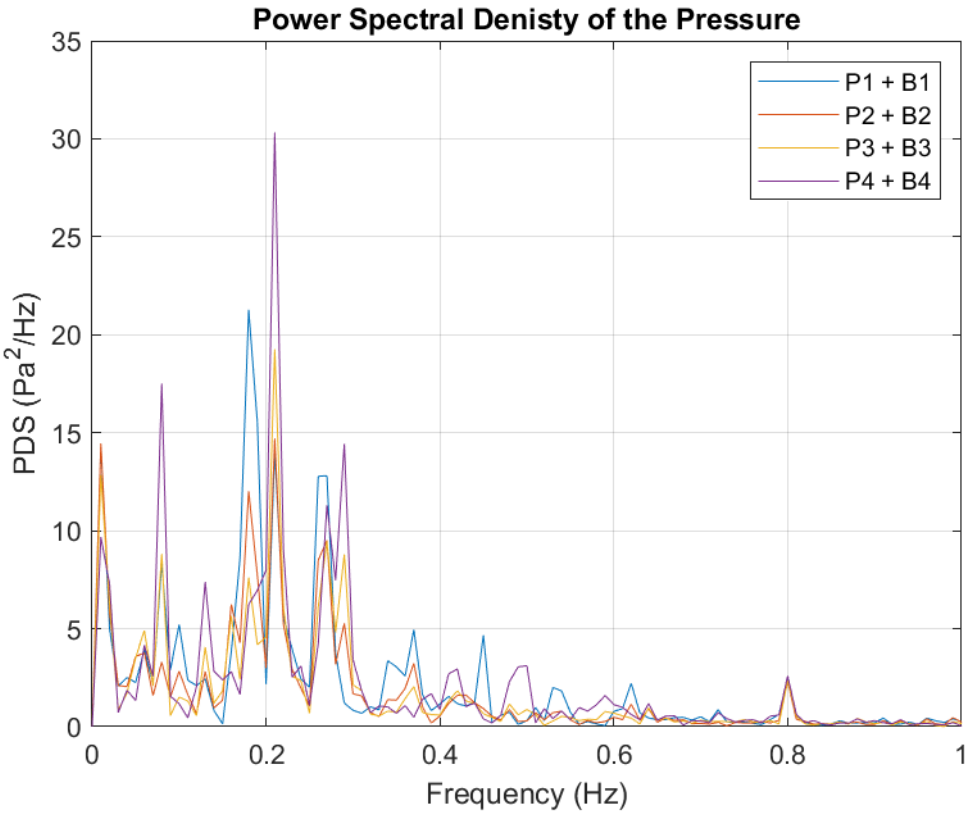

Figure 4.16 Power Spectral Density of the pressure for the second 3D simulation

Table 4.4 Mean pressure values per pressure point for the second 3D simulation

Point	Mean Pressure q_μ (Pa)	Standard deviation of the Pressure q_σ (Pa)
P1 + B1	1035	31
P2 + B2	1275	23
P3 + B3	1274	24
P4 + B4	1034	34

The power spectral density in Figure 4.16 shows a clear peak at 0.2 Hz (~5 sec). A few other peaks are present in the data, but these peaks with a higher frequency are not significant. The data shows that the outer edges, P1 and P4, show more fluctuations than the inner edges P2 and P3, which was as expected.

Comparison of the 2D and the 3D simulation

The results obtained from the 2D and the 3D simulation on the windward side show differences; these differences are shown in Table 4.5.

Table 4.5. Summarized results of CFD simulations

	2D simulation (Pa)			3D simulation (Pa)		
Point	Mean pressure q_μ	Standard Deviation of the pressure q_σ	Peak velocity Pressure q_p	Mean pressure q_μ	Standard Deviation of the pressure q_σ	Peak velocity Pressure q_p
P1	563	173	1169	518	30	623
P2	1022	65	1250	764	30	869
P3	1023	84	1317	764	30	869
P4	560	219	1327	518	31	627

From these results, it can be concluded that the 3D simulations give significantly lower values. The reason can be found in the development of the air in height, which is restricted for the 2D simulation. The 3D simulation allows the wind to diverge in height which brings other effects into account.

4.3 Comparison between spectral approach and CFD results

A comparison of the results of the spectral approach and the CFD simulations is made. The results of the pressure over time are presented in Table 4.6.

Table 4.6 Results of CFD simulations and spectral approach summarized, pressure in Pa

Point	**3D simulation (Pa)**			**Spectral approach (Pa)**		
	Mean pressure q_μ	Standard Deviation of the pressure q_σ	Peak velocity Pressure q_p	Mean pressure q_μ	Standard Deviation of the pressure q_σ	Peak velocity Pressure q_p
P1+B1	1035	31	1144	781	279	1611
P2+B2	1275	23	1356	781	279	1611
P3+B3	1274	24	1358	781	279	1611
P4+B4	1034	34	1153	781	279	1611

An important difference in the input of the CFD simulations and the spectral approach is the air's different density. To compare the results with the same density, the CFD results are transformed from an air density of $1.18\ kg/m^3$ to an air density of $1.25\ kg/m^3$. For clarity only the peak velocity is presented in Table 4.7.

Table 4.7 Results of the peak velocity of the 3D CFD simulation and the spectral approach with a similar air density

Point	**Peak velocity Pressure 3D simulation $q_{p,3D}$ (Pa)**	**Peak velocity Pressure of the Spectral Approach $q_{p,SA}$ (Pa)**	**Difference $\left(\frac{q_{p,SA} - q_{p,3D}}{q_{p,SA}}\right) \cdot 100\%$**
P1+B1	1211	1611	24,8
P2+B2	1435	1611	10,9
P3+B3	1438	1611	10,7
P4+B4	1221	1611	24,2

It can be concluded that the results of the 3D CFD simulation underpredict the wind pressure when comparing with the spectral approach. It is generally known that a lot of conservative assumptions and statistics are present in the used wind spectra, and this is not included in the CFD input. The input of the CFD simulation is formulated with a range of the turbulent kinetic energy and an adaptive function. This means that the turbulence is calculated per cell. Therefore, it is hard to formulate a clear image of the incoming wind turbulence with this turbulent kinetic energy range.

The CFD simulations are performed with the U-RANS method, which only captures slow turbulences. This could explain the difference between the amplitude of the standard deviation of the CFD simulations and the spectral approach.

The power spectral density function of the results show clear peaks around 0.2 Hz. This is close to the structure's eigenfrequency, which is mainly of importance when researching the structural dynamics. For this thesis no further CFD simulations are performed, but it is recommended for further studies to validate the CFD data better with existing literature.

Discussion

In this research, different choices and assumptions are made for numerous reasons. The most critical issues are elaborated and discussed, including the effect on the final result.

The research started with limited available knowledge about wind and CFD simulations. Engineering Company ABT B.V. provided the CFD simulations with formulated input. Beforehand, it was not clear what was expected and what information was needed to gain relevant results. ABT did have experience for hindrance simulations, but did not use CFD simulations for wind loads. It was their goal to learn about such a procedure. CFD simulations performed by an external company are time-consuming and expensive, so the provided results could not be improved time after time. The different parties made assumptions, which was only noticed later, e.g. a different chosen air density. These differences could be found in the input file of the concerning simulation, and these files contain numerous technical details of the assumptions made. More knowledge about CFD would differ in understanding the files and would improve the communication about the input and the results.

The first validation of the CFD simulations was done on a reference structure with available wind tunnel data. Extensive wind-tunnel data is rarely available online since this is a costly procedure which is often performed for case-specific situations for commercial parties. The data used from the Tokyo Polytechnical University shows a lot of noise, which is not preferable. The data of other pressure tapes located at different heights did not give more precise results. The database contains many different results, but the circumstances of the input and the boundaries are hard to find and reproduce. Other data could be cleaner, which would have resulted in more clear frequency dependency. Better available information of the circumstances would improve the simulation process to ensure similar input was used.

The goal of analysing the wind tunnel data was to validate the CFD simulation on a similar reference structure. At the beginning of the research, this validation was insufficiently made. The period of the fluctuating pressure coefficients was only partly reproduced, and the absolute values of both tests did not coincide. However, a similar CFD procedure was used for the full-scale case study. With the current knowledge, it is concluded that more effort would have had to be made to assume this validation to be sufficient. Due to a restriction of time, this first validation has not been improved. In further research, this should be improved.

The full-scale case study was simulated with a spectral approach and CFD simulations. For the spectral method assumptions are made regarding the input. Multiple complex functions could not analytically be solved with the software MATLAB. Therefore, approximations for discretizations are made to obtain the aerodynamic admittance. More advanced software could solve the expressions analytically, which would result in a more exact outcome.

In the spectral approach, the deformed shape of the structure is included in the simulation. Only the first mode shape is used in the calculation, which represents a parabolic deformation. For a complete result, different mode shapes should be included.

The deformed shape of the structure is not included in the CFD simulations. In the CFD simulation the building is modelled as an endless rigid block, so no fluid-structure interaction is implemented. However, in the spectral approach, the fluid-structure interaction is partly included.

The case study CFD simulations results are only extracted at the height of 150 meters and averaged over 10 x 10 meters. Results on multiple elevation levels would give a better idea of the total loading on the structure. Choosing a smaller area where the results are averaged, would result in a more accurate outcome. When the average is taken over 100 m^2, fluctuations

within that area are balanced out. A smaller size would result in better results, especially when only the averaged values are used.

Finally, this research describes only the along- wind direction with wind coming at an angle of 0°. The across-wind direction gives a better view of the development of the vortices. Changing the wind direction would also lead to more results so that parametric studies could be achieved.

Conclusions

The dynamic wind loading is used as an equivalent static loading in the current strength calculations. The use of CFD could provide more insight into the dynamic part of the wind loading. At the moment, the Eurocode states that CFD simulations cannot be used for strength calculations. As formulated in Chapter 1.2, the research aims to create a validation methodology for the reliability of CFD results. The sub-research questions are first answered to found the answer to the main research question. Finally, recommendations for further research are presented.

5. Conclusions

5.1 Sub-research questions

- *What assumptions have to be made and which output is needed from CFD simulations?*

The basic principle from CFD simulations is solving the Navier-Stokes (NS) equations. Solving these coupled nonlinear differential equations results in a fluid flow behaviour description. Building such a simulation requires various steps. First of all, a finite computational domain needs to be formulated since this bounds the field of interest. Appropriate boundaries must be defined at suitable locations. The boundaries have different properties affecting the fluid flow. An incoming velocity profile defines the inlet boundary with a coherent turbulence intensity profile. A pressure outlet defines the outlet boundary. The ground floor is defined as a no-slip boundary, which means that the ground level's velocity is equal to zero. The top of the domain is a symmetry condition. The walls are slip boundaries, which means that the fluid flow is parallel in the windward direction to the surface. The locations of the boundaries can be designed according to practical guidelines, which ensure that the effect of the walls are desirable on that location. This means that the wall- and top surfaces are located at a significant distance from the structure(s) of interest. The distance between the inlet boundary guarantees a stabilised fluid flow, with the effect of the ground roughness included, when the flow reaches the model of interest. The outlet boundary has a distance far enough from the model to assure a development, including stabilising the model's fluid flow.

The total domain is divided by a mesh of cells, where for every cell the NS equations is solved by using different schemes depending on defined time steps. A mesh refinement has to be implemented in the areas of interest to acquire accurate results. Various methods, with varying costs, are available to run the simulations. This research uses the Reynolds-Averaged Navier-Stokes (RANS) model, with an extension of the Unsteady RANS (U-RANS) model. This RANS model's basis lies in solving the NS equations for the steady-state solution, where the U-RANS also captures the slow turbulences.

The structure of interest must define the locations of interest before the simulation performs. Pressure values are averaged on a provided area, and the data is stored while running the simulation. When these locations are not defined beforehand, the simulation has to run again to save these data. The simulations require significant computational power, so the simulations are run on an external server. Only running the simulation costs a substantial amount of calculation time. The calculation time of the simulations performed for this research varies from 14 hours until almost two days.

- *How do the CFD results have to be validated?*

When a regular CFD simulation is used for wind load calculations on a structure, the results are validated with wind tunnel data. The data can be compared based on pressure values and the coherent standard deviation. Different parameters, such as different model geometries and other wind directions, have to be changed, and the results of both the CFD simulation and the wind tunnel data can be compared. The data can also be converted to the frequency domain to see if the power spectral density functions coincide.

In this research an attempt is made to validate the CFD results with existing available wind tunnel data. Both simulations show a period around 0.1 seconds, corresponding with a frequency of around 10 Hz. The wind tunnel data shows however more fluctuations and more irregularity. However, the validation is not sufficient since significant differences are present in both the mean value of the pressure, the standard deviation of the pressure and the power spectral density function. Reasons for this difference can be found in both the wind tunnel data and the CFD simulation. The wind tunnel pressure date contains extraordinary fluctuations in amplitude and frequency ranges. On the other hand, the CFD data shows a straightforward result, only one dominant frequency can be observed from the results. Due to a restriction of time, no extra validations are performed.

- *How can the CFD results be compared with a turbulence spectrum approach?*

The CFD results and the turbulence spectrum approach can be compared by comparing the mean pressure on the surface and its coherent standard deviation. For the case study a reference model of 40 x 40 x 200 is meters used. A spectral approach analyses is executed and validated with existing literature. For the CFD simulations different methods are used. First, a semi-2D simulation is set up. Only the wind velocity on a 10 meter thick plate on a height of 150 meters over the domain is monitored. The wind velocity on other elevation levels is not simulated. Afterwards, two 3D simulations were performed. The result of the first 3D simulation damped out over time, which is not trustworthy. The reason for this was found in the resolution of the results, increasing the plot sample of the results solved this issue in a second 3D simulation. This simulation gave clear results; the pressure data converged to a stable oscillating pattern. The results of the second 3D simulation are combined to include both the pressure directly caused by the wind and the effect of the wake behind the structure. The values of the mean pressure were in the same range, but the standard deviation of the pressure was significantly lower for the CFD simulation. In the CFD simulation, the pressure is averaged over 100 m^2, which balances out a lot of turbulence. This could explain the lower standard deviation.

The power spectral density translates the fluctuating component in the time domain to the frequency domain. The spectral approach results have a wind turbulence spectrum as input, with lots of statistics included. The CFD simulations' input is restricted to only a velocity profile and an adaption criterion function to approximate the turbulence kinetic energy; therefore, the power spectral density functions are hard to compare.

5.2 Main research question

The main research question was:

What is the impact of various parameters in an analyse of the dynamic loading on a high-rise building resulting from wind loading by using CFD simulations?

The simulation procedure and the coherent assumption defining the reality are of great importance for an analysis of the dynamic loading on a high-rise structure. The location and properties of boundary conditions are generally relatively simple to implement when using

practical guidelines for CFD simulations. The used model depends on the purpose of the simulation and the available time and finances. For this research is the U-RANS model used, which is an extension of the RANS model. Where the RANS model computes the steady-state solution of a simulation, the U-RANS model includes slow turbulences in the simulation. For the relevant frequencies, the frequencies close to the natural frequencies, for a high-rise building load, it was expected that the U-RANS could capture these physics. It is visible that the frequencies below 1 Hz are present in the results, which corresponds to the frequency range of interest. The absolute values of the pressure are comparable, but the standard deviation of the CFD results did not coincide with the values obtained from the spectral approach. Reasons for this can be found in the incoming wind properties, which are not exactly equal in both analyses. The spectral approach uses a wind spectrum including lots of statistics and conservatism. The CFD simulation approximates the turbulences with an adoptive turbulent kinetic energy criterion function. Also, the pressure results are the average over a 10 x 10 meter area, which is an extreme size for such an output. Smaller fluctuations are balanced out on an area of 100 m^2. When an area of 1 m^2 would be used to take the average pressure, the standard deviation of the wind pressure will increase to more realistic values.

Recommendations

CFD simulations are complex, and a lot of variety in accuracy is present in different kind of simulations. Some results are very elaborate, and others are more simple. For this study only limited analyses are performed, with no CFD experience in simulating wind loads beforehand. The results were obtained by a lot of improvements and reconsiderations. Since another person performed the simulations, some assumptions were made that should differ from the knowledge gained a few months later. However, for this study's scope and the limited amount of time, not all simulations were improved. For further studies, it is recommended to perform the CFD simulations yourself, to know exactly what is used and assumed as input. It also gives a bit more flexibility when new analyses have to be performed.

The wind tunnel data used for the validation shows a lot of noise and is therefore hard to reproduce with the available information. Other wind tunnel data is recommended to validate CFD simulations in the future.

In this study only the wind pressure on the windward façade was analysed, data of the other directions could lead to interesting results.

The spectral approach is applied in the case study. This method includes the mode shape of the structure. In the CFD simulation a rigid structure is modelled. A fluid-structure interaction model would provide significant insights into the use of CFD for a dynamic wind load on high rise buildings.

References

Abubaker, A., Kostić, I., & Kostić, O. (2018). Numerical modelling of velocity profile parameters of the atmospheric boundary layer simulated in wind tunnels. *IOP Conference Series: Materials Science and Engineering*, *393*(1). https://doi.org/10.1088/1757-899X/393/1/012025

Amin, J. A., & Ahuja, A. K. (2013). Effects of Side Ratio on Wind-Induced Pressure Distribution on Rectangular Buildings. *Journal of Structures*, *2013*, 1–12. https://doi.org/10.1155/2013/176739

Announcement of the Alan G. Davenport Wind Loading Chain. (2011). *Journal of Wind Engineering and Industrial Aerodynamics*. https://doi.org/10.1016/j.jweia.2011.09.005

CCM User Guide- star- CD version 4.02. (2006).

Clannachan, G. H., Lim, J. B. P., Bicanic, N., Taylor, I., & Scanlon, T. J. (2009). *Practical Application of CFD for Wind Loading on Tall Buildings*. (January), 767–776. https://doi.org/10.3850/9789628014194_0072

Epinette, J., & Sutton, K. (2003). *Fluent 6.1 User's Guide*. Lebanon.

Franke, J., Hellsten, A., & Carissimo, B. (2007). Best practice guideline for the CFD simulation of flows in the urban environment. In *Journal of Gastrointestinal Surgery*. https://doi.org/10.1016/S1091-255X(01)80095-0

Fröhlich, J., & Rodi, W. (2004). LES of the flow around a circular cylinder of finite height. *International Journal of Heat and Fluid Flow*, *25*(3), 537–548. https://doi.org/10.1016/j.ijheatfluidflow.2004.02.006

Hagos, A., Habte, F., Chowdhury, A. G., & Yeo, D. (2014). Comparisons of two wind tunnel pressure databases and partial validation against full-scale measurements. *Journal of Structural Engineering (United States)*, *140*(10), 1–14. https://doi.org/10.1061/(ASCE)ST.1943-541X.0001001

Luo, Y., Liu, H., Xue, H., & Lin, K. (2019). Large-eddy simulation evaluation of wind loads on a high-rise building based on the multiscale synthetic eddy method. *Advances in Structural Engineering*, *22*(4), 997–1006. https://doi.org/10.1177/1369433218794258

Ricci, M., Patruno, L., Kalkman, I., de Miranda, S., & Blocken, B. (2018). Towards LES as a design tool: Wind loads assessment on a high-rise building. *Journal of Wind Engineering and Industrial Aerodynamics*, *180*(2018), 1–18. https://doi.org/10.1016/j.jweia.2018.07.009

Rusdin, A. (2017). Computation of turbulent flow around a square block with standard and modified k-ε turbulence models. *International Journal of Automotive and Mechanical Engineering*, *14*(1), 3938–3953. https://doi.org/10.15282/ijame.14.1.2017.10.0320

Shaheed, R., Mohammadian, A., & Kheirkhah Gildeh, H. (2019). A comparison of standard k–ε and realizable k–ε turbulence models in curved and confluent channels. *Environmental Fluid Mechanics*, *19*(2), 543–568. https://doi.org/10.1007/s10652-018-9637-1

Simiu, E., & Scanlan, R. H. (1986). *Wind effects on structures*.

Standard, E. (2005). *Eurocode 1: EN 1991-1-4: Actions on structures - Part 1-4: General actions - Wind actions*.

Steenbergen, R. D. J. M., Vrouwenvelder, A. C. W. M., & Geurts, C. P. W. (2012a). The use of Eurocode EN 1991-1-4 procedures 1 and 2 for building dynamics, a comparative study. *Journal of Wind Engineering and Industrial Aerodynamics*. https://doi.org/10.1016/j.jweia.2012.03.025

Steenbergen, R. D. J. M., Vrouwenvelder, A. C. W. M., & Geurts, C. P. W. (2012b). The use of Eurocode EN 1991-1-4 procedures 1 and 2 for building dynamics, a comparative study. *Journal of Wind Engineering and Industrial Aerodynamics*, *107–108*, 299–306. https://doi.org/10.1016/j.jweia.2012.03.025

Tamaru, Y., & Quan, Y. (2007). *Aerodynamic database for non-isolated low-rise buildings*. Tokyo.

Tamura, Y. (Tokyo P. U. (2012). Aerodynamic Database of High-rise Buildings.

Tamura, Y., & Kareem, A. (2013). Advanced structural wind engineering. In *Advanced Structural Wind Engineering*. https://doi.org/10.1007/978-4-431-54337-4

Ted Stathopoulos, C. C. B. (2007). Wind Effects on Buildings and Structures. *Nature*, *199*(4898), 1049–1050. https://doi.org/10.1038/1991049a0

Tominaga, Y. (2015). Flow around a high-rise building using steady and unsteady RANS CFD: Effect of large-scale fluctuations on the velocity statistics. *Journal of Wind Engineering and Industrial Aerodynamics*, *142*, 93–103. https://doi.org/10.1016/j.jweia.2015.03.013

Tu, J., Yeoh, G.-H., & Liu, C. (2018). Practical Guidelines for CFD Simulation and Analysis. In *Computational Fluid Dynamics*. https://doi.org/10.1016/b978-0-08-101127-0.00007-6

Vrouwenvelder, A. C. W. M. (2004). *Lecture notes CT5145: Random Vibrations*. https://doi.org/10.1016/S0920-3796(88)80003-6

Zielińska, M., & Zarychta, K. (2015). A comparison of the wind spectrum according to different methods-an original project of a building on a cliff in Gdynia. *International Journal of Applied Mechanics and Engineering*, *20*(3), 663–672. https://doi.org/10.2478/ijame-2015-0045

Appendices

Appendix A- Monte Carlo Simulation

The aerodynamic admittance can be computed with a Monte Carlo simulation. The Monte Carlo simulation uses random generated samples between boundaries to approximate a surface integral. In this case, 2^{16} samples are used to estimate the integral of the aerodynamic admittance according to the following formula.

$$X^2_{\Phi_i}(n) = \frac{1}{A^2}\int_h\int_h\int_b\int_b \frac{v_{m,k}}{v_{m,z_s}}\frac{v_{m,l}}{v_{m,z_s}}\,\Phi_i(y_k,z_k)\,\Phi_i(y_l,z_l)\,coh_{v_k v_l}(n)\,dy_k dy_l dz_k dz_l$$

The frequency range is formulated between 10^{-3} and 10 Hz, with corresponding n_{steps}. For every frequency within the range, the $X^2_{Monte\ Carlo}(n)$ is calculated. This is done by generating random samples for z_k, z_l, y_k and y_l by multiplying the boundaries by the $rand$- function in MATLAB. The $rand$-function provides a random number between 0 and 1. This results, for example, for $z_{k_{random}}$ in values between 0 and the total height of the structure. A double loop is used to obtain results over the different frequencies.

$$Nsample = 2^{16}$$
$$n_{steps} = logspace(-3{,}1{,}100)$$
$$coh(n,z_k,z_l,y_k,y_l) = e^{\frac{-2\cdot n}{v_m(z_k)+v_m(z_l)}\cdot\sqrt{C_z^2\cdot(z_k-z_l)^2+C_y^2\cdot(y_k-y_l)^2}}$$
$$innerfunction(n,z_k,z_l,y_k,y_l) = \frac{v_m(z_k)\cdot v_m(y_k)}{v_m(z_s)^2}\cdot\Phi_1(z_k)\cdot\Phi_1(z_l)$$
$$for\ x = 1:length(n_{steps})$$
$$inner(z_k,z_l,y_k,y_l) = innerfunction(n_{steps}(x),z_k,z_l,y_k,y_l)$$
$$for\ i = 1{:}\,Nsample$$
$$z_{k_{random}} = h\cdot rand$$
$$z_{l_{random}} = h\cdot rand$$
$$y_{k_{random}} = b\cdot rand$$
$$y_{l_{random}} = b\cdot rand$$
$$inner_x(i) = coh(n,z_k,z_l,y_k,y_l)\frac{v_m(z_k)\cdot v_m(y_k)}{v_m(z_s)^2}\cdot\Phi_1(z_k)\cdot\Phi_1(z_l)$$
$$end$$
$$mean(x) = mean(inner_x)$$
$$end$$
$$X^2_{Monte\ Carlo}(n) = mean\,(mean(x))$$

Appendix B – Spectral Approach

The spectral approach is applied with the use of the computer program MATLAB. The procedure as stated in Chapter Spectral approach2.3 Spectral approach is used. Due to the complexity of some formulas, assumptions are made. These assumptions are made to discretize some formulas. The dependency of the frequency required discretizations in some formulas. These formulas are stated in this appendix.

The calculation starts with a wind spectrum as input. The spectrum of Solari is used according to the Eurocode. Wind spectra are usually defined as a dimensionless function. With the turbulence length scale on the reference height $L(z_s)$ and the mean wind speed $v_m(z_s)$ is the dimensionless frequency $f_L(n)$ calculated. The wind spectrum $S_{vv}(n)$ is computed with the dimensionless spectrum of Solari, the standard deviation of the wind velocity $\sigma_v(z_s)$ and is depending on the frequency n.

$$f_L(n) = \frac{n \cdot L(z_s)}{v_m(zs)}$$

$$S_L(n) = \frac{6.8 \cdot f_L(n)}{\left(1 + 10.2 \cdot f_L(n)\right)^{5/3}}$$

$$S_{vv}(n) = \frac{S_L(n) \cdot \sigma_v(z_s)}{n}$$

The discretization to obtain the aerodynamic admittance is made by defining a dz value. This value defines the size of the separate areas, resulting in a mesh in y direction and in z direction over the surface. Afterwards, the total surfaces n_{tot} are computed.

$$dz = 2.5\ meters$$

$$dz_k = dz_l = dy_k = dy_l = dz$$

$$mesh_y = \frac{b}{dz} \ and \ mesh_z = \frac{h}{dz}$$

$$n_{tot} = mesh_y \cdot mesh_z$$

The different results in further calculations are dependent on the frequency n. A frequency range is defined to limit the amount of computational time. The aerodynamic admittance ${X(n)_{\Phi_1}}^2$ is computed with the sum of the different results per mesh area. The load spectrum $S_{FF}(n)$ on the structure is calculated by combining the formulas according to Chapter Spectral approach2.3 Spectral approach.

$$n = logspace(-3,1,100)$$

$$coh(n, z_k, z_l, y_k, y_l) = \mathrm{e}^{\frac{-2 \cdot n}{v_m(z_k) + v_m(z_l)} \cdot \sqrt{C_z^2 \cdot (z_k - z_l)^2 + C_y^2 \cdot (y_k - y_l)^2}}$$

$${X(n)_{\Phi_1}}^2 = \sum_{k=1}^{i} \sum_{l=1}^{j} \frac{v_{m,k} \cdot v_{m,l}}{v_{m,z_s}^2} \Phi_1(y_k, z_k) \cdot \Phi_1(y_l, z_l) \cdot coh(n, z_k, z_l, y_k, y_l) \cdot dz_k \cdot dy_k \cdot dz_l \cdot dy_l$$

$$H_a(n) = \rho \cdot c_f \cdot v_m(z_s) \cdot A \cdot X(n)^2$$

$$S_{FF}(n) = S_{vv}(n) \cdot |H_a(n)|^2$$

Appendix C - Fourier transform

A Fourier transform is a mathematical method that connects a time sampled signal to a same signal sampled in frequency.

$$F(\omega) = \frac{1}{\sqrt{2\,\pi}} \int_{-\infty}^{\infty} f\,(t) e^{-i\omega t}\, dt$$

$F(\omega)$ represents the signal in the frequency domain and $f(t)$ represents the signal in the time domain. When a continuous signal is available, the previous expression can be used to transform the signal from the time-domain to the frequency-domain. A signal consisting of discrete data can be transformed with a Discrete Fourier Transform (DFT) algorithm. The Fast Fourier Transform (FFT) algorithm is an optimized application of the DFT algorithm. The FFT algorithm is used for this research to obtain the power spectral density as a function of the frequency.

Appendix D – Comparison of Wind tunnel data

Since the wind tunnel data show a lot of noise, an extra check is being done by comparing the data with another dataset. Only the $C_p\ mean$, the $C_p\ max$ and the $C_p\ min$ are available from this dataset unfortunately. Therefore only the absolute values of these coefficients can be checked, this doesn't give an explanation of the amount of noise.

In both the Tokyo Polytechnic University and the Indian Institute of Technology is a model of 100 x 100 x 300 mm placed in a wind tunnel. Both institutes had a different incoming wind speed and different turbulence intensities, but the dimensionless pressure coefficient can be compared. This is done by taking all pressure tabs on the different tabs per face of the building. The results of the different faces are compared in Table 5.1.

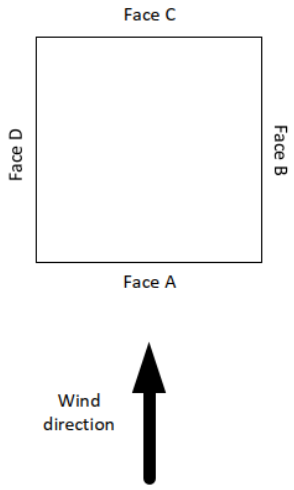

Figure 5.1 Setup wind tunnel data and coherent faces

Table 5.1 Comparison of results of different wind tunnel experiments

		Face A	Face B	Face C	Face D
Tokyo Polytechnic University (Y. (Tokyo P. U. Tamura, 2012)	**Cp mean**	0,54	-0,82	-0,54	-0,84
	Cp max	0,88	-0,43	-0,47	-0,4
	Cp min	0,14	-1,05	-0,64	-1,07
Indian Institute of Technology (Amin & Ahuja, 2013)	**Cp mean**	0,74	-0,69	-0,5	-0,69
	Cp max	1,11	-0,6	-0,59	-0,6
	Cp min	0,25	-1,1	-0,9	-1,05
Eurocode (Standard, 2005)	**Cp**	0,8	-1,2/-0,8	-0,7	-1,2/-0,8

From these results, it is noticed that negative values of mean values of the Eurocode are lower than the experimentally observed values. The positive pressure coefficient of the wind tunnel data are lower than the Eurocode.

Appendix E – Analysis of first 3D simulation

The 3D simulations also have data stored on the backside of the structure, B1 till B4. The results are shown in Figure 5.2. An increase in the results is observed over time. Based on these observations, it can be concluded that there is no convergence of the simulation.

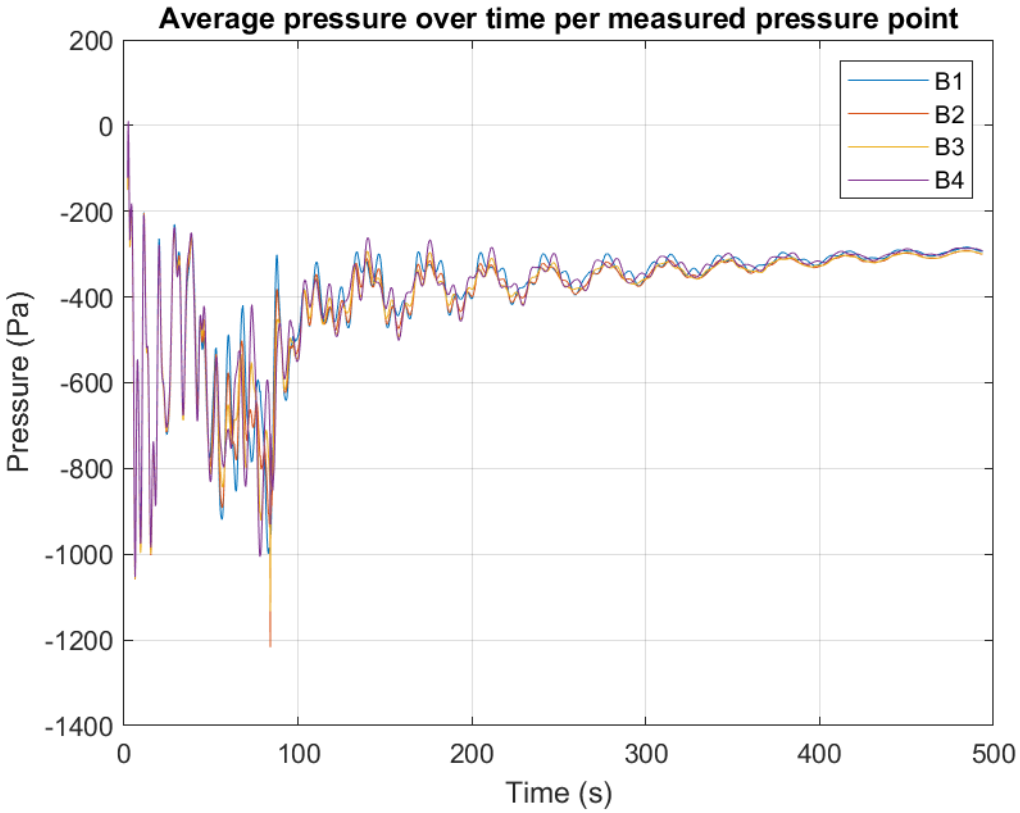

Figure 5.2 Pressure over time of the backside from the first 3D CFD simulation

When the pressure over the different area is summarized per part, the results provide more insight into the simulation process. The summarized results are presented in Figure 5.3.

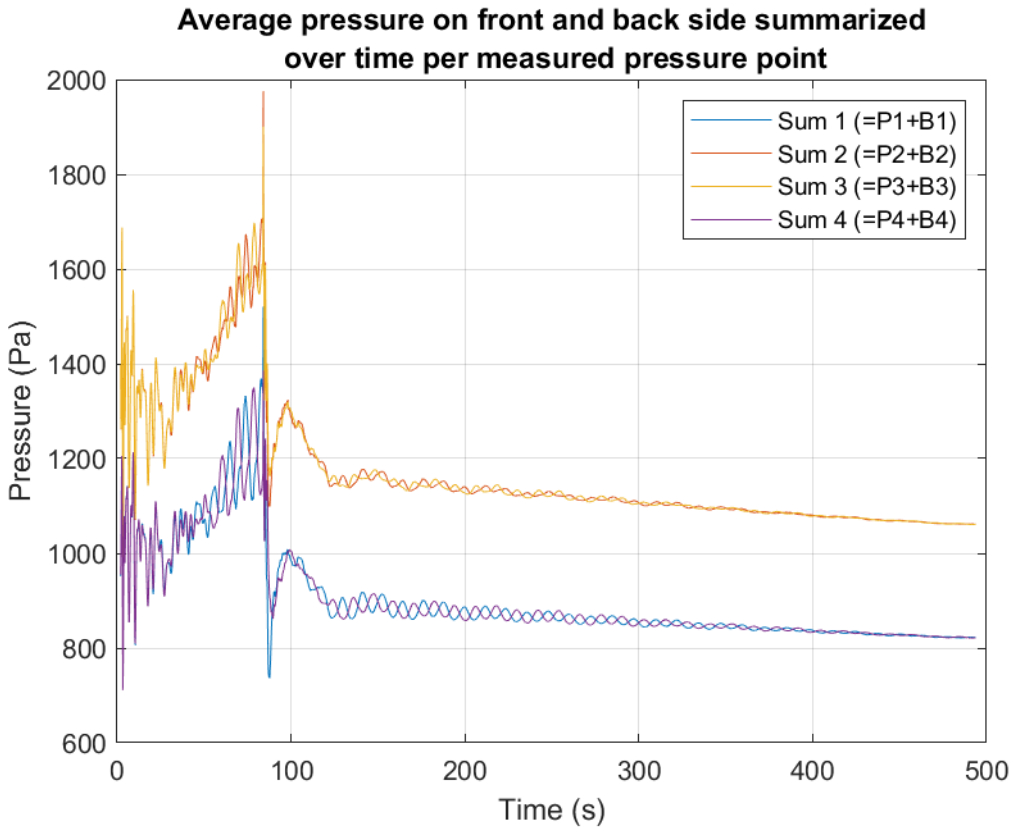

Figure 5.3 Summarized results of the first 3D CFD simulation

The results can be described with three different phases in the simulation. The first phase is from 0 to 90 seconds; here the initial conditions are determined. When a simulation starts, the domain cells are empty; they don't contain information regarding the air velocity or the pressure. In the first phase these cells are filled with values according to the traditional RANS method, so only a steady-state solution is made. In the second phase, at the drop at 90 seconds, the RANS simulation changes to the U-RANS simulation. Now the turbulence is added more specifically. The third phase can be observed from 100 seconds till 500 seconds, the slow turbulences are captured here. For the U-RANS phase, a plot sample of 20.000 values was used. It appeared that this plot sample did not give the right physics; more resolution was needed in the results. The plot samples for the second 3D simulations are therefor increased to 50.000, which provides better results.

Appendix F – Development of the 3D simulation

For the second 3D simulation, the results of the semi-2D simulation are used as initial conditions. The semi-2D simulations only simulated the wind velocities in a strip of 10 meters thick on a height of 150 meters. The average of these results is extended over the height and used as initial conditions. For all figures shown below, the vorticity is visualised in the upper left-, the lower left and the lower right figure. In the upper right figure is the pressure of the areas P1 till P4 presented over time.

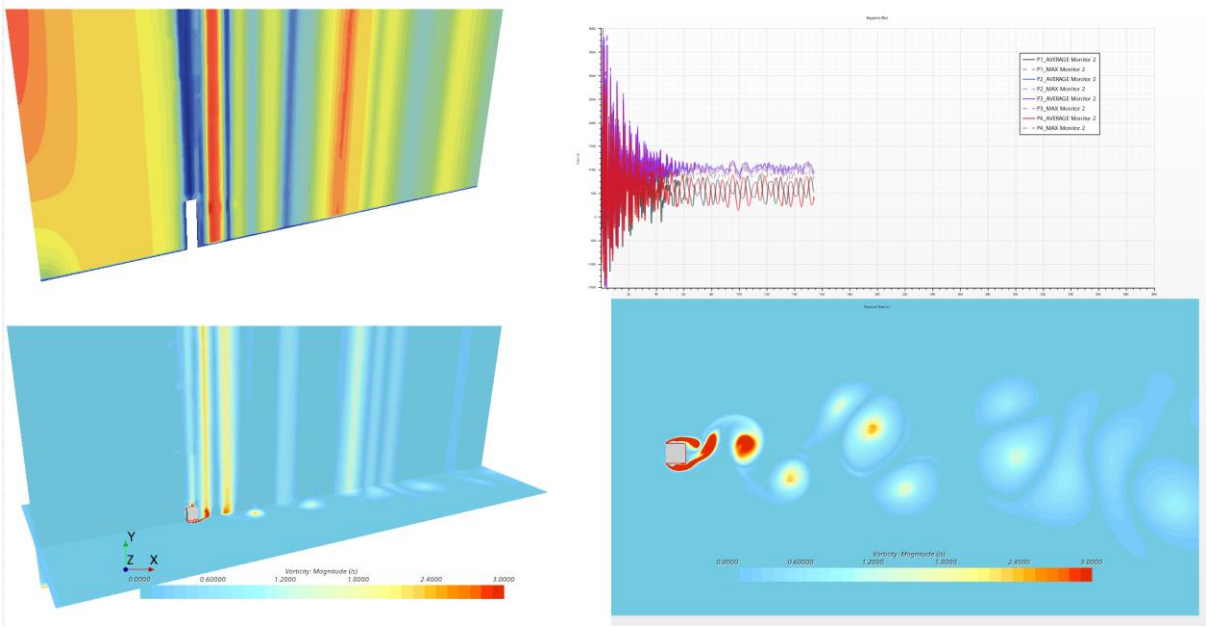

Figure 5.4 Overview of the start of the second 3D simulation at t=180 seconds.

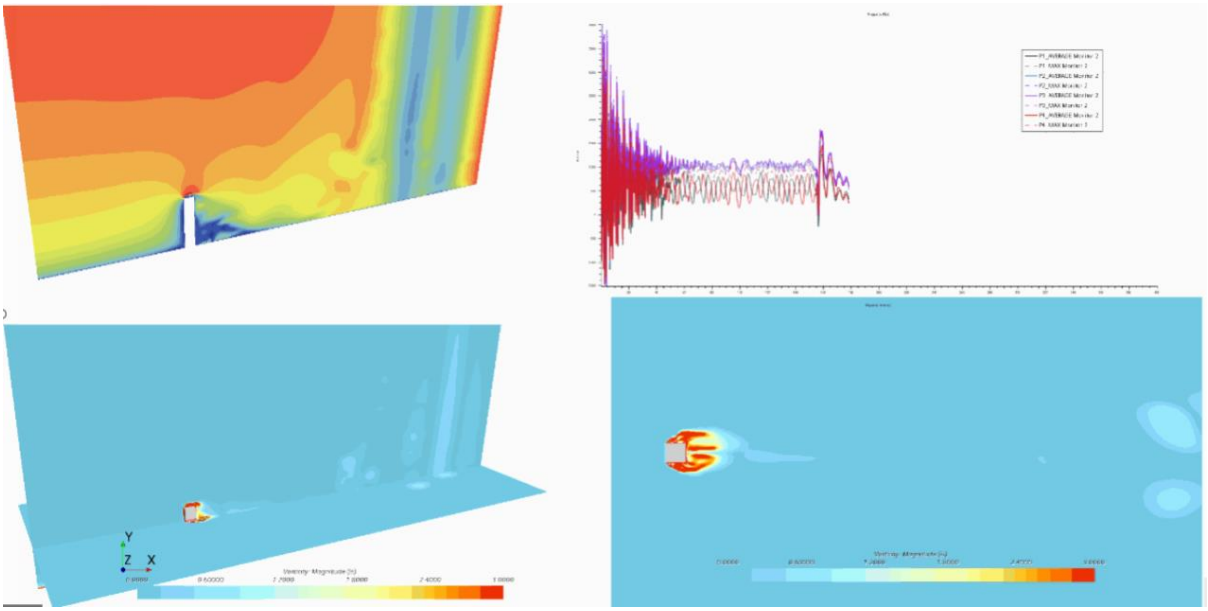

Figure 5.5 Overview second 3D simulation at t=190 seconds

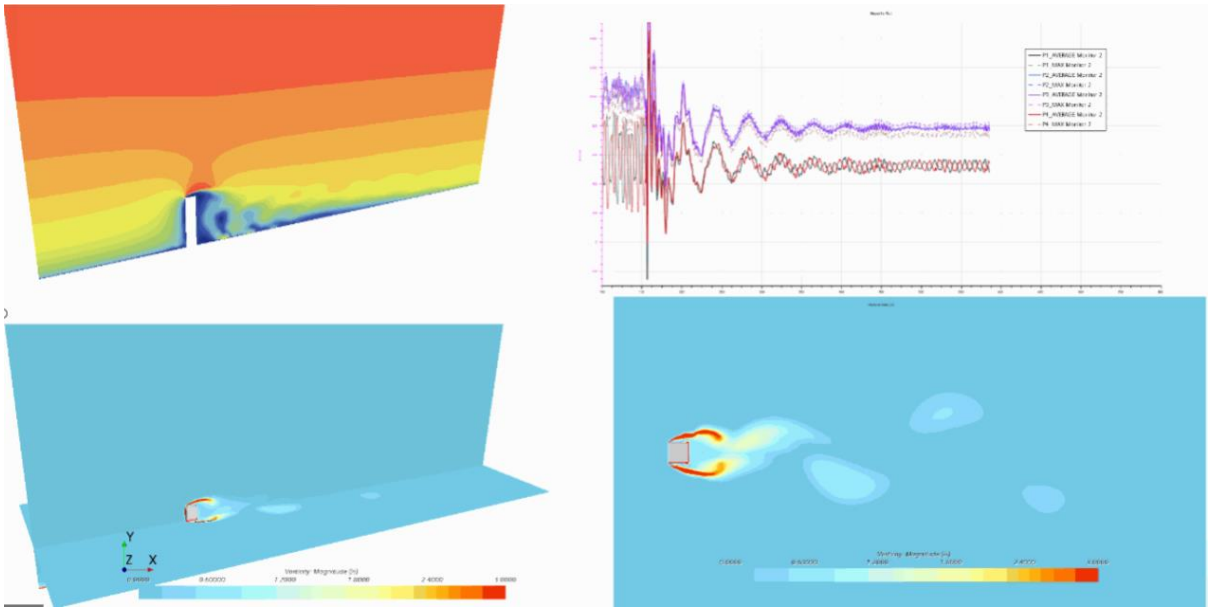

Figure 5.6 Overview second 3D simulation at t=550 seconds